SPACS: A semi-empirical parameterization for isotopic spallation cross sections

C. Schmitt,[1] K.-H. Schmidt,[1] and A. Kelić-Heil[2]
[1]*Grand Accélérateur National d'Ions Lourds, CEA/DSM-CNRS/IN2P3, Boîte Postale 55027, 14076 Caen, France*
[2]*GSI-Helmholtzzemtrum für Schwerionenforschung GmbH, 64291 Darmstadt, Germany*
(Received 11 July 2014; revised manuscript received 27 October 2014; published 3 December 2014)

A new semi-empirical parameterization for residue cross sections in spallation reactions is presented. The prescription named SPACS, for spallation cross sections, permits calculating the fragment production in proton- and neutron-induced collisions with light up to heavy non-fissile partners from the Fermi regime to ultra-relativistic energies. The model is fully analytical, based on a new parameterization of the mass yields, accounting for the dependence on bombarding energy. The formalism for the isobaric distribution consists of a commonly used functional form, borrowed from the empirical parameterization of fragmentation cross sections EPAX, with the observed suited adjustments for spallation, and extended to the charge-pickup channel. Structural and even-odd staggering related to the last stage of the primary-residue deexcitation process is additionally explicitly introduced with a new prescription. Calculations are benchmarked with recent data collected at GSI, Darmstadt as well as with previous measurements employing various techniques. The dependences observed experimentally on collision energy, reaction-partner mass, and proton-neutron asymmetry are well described. A fast analytical parameterization, such as SPACS, can be relevant to be implemented in complex simulations as used for practical issues at nuclear facilities and plants. Its predictive power also makes it useful for cross-section estimates in astrophysics and biophysics.

DOI: 10.1103/PhysRevC.90.064605 PACS number(s): 25.40.Sc, 25.40.Kv, 24.10.−i, 25.70.Mn

I. INTRODUCTION

Fragmentation and spallation reactions[1] are customarily used to produce exotic nuclei for studying their properties and possibly exploit them as secondary projectiles. Today, there is growing interest in the specificities of the spallation process. A large part of existing and future radioactive-beam facilities (see, e.g., Refs. [1–3]) is based on proton beams impinging on a heavy target material. Spallation reactions, induced by either protons or neutrons, are also the cornerstone in accelerator-driven subcritical reactors [4,5]. They play a key role in astrophysics along the propagation of cosmic-ray nuclei in the interstellar medium (consisting of 93% of hydrogen) and, in turn, in explosive nucleosynthesis processes [6]. Finally, the relevance of spallation in biophysics [7], namely, for medical purposes, is established.

For optimizing the parameters of a physics experiment, controlling a nuclear-energy installation, computing stellar abundances, or adapting a nuclear-therapy treatment to specific organs, a solid knowledge of the fragment production by either proton- or neutron-induced spallation is necessary. Elaborate simulations performed with programs, such as, e.g., MARS15 based on former LAHET [8], MCNP6 [9], or FLUKA [10], are used to predict the physics of primary and secondary processes by means of coupling an intranuclear cascade code and a deexcitation model [11,12] as well as they do follow the transport of the final products, including light particles and photons, in the complex experimental environment (see, e.g., Ref. [13] in astrophysics). As the complete simulation can be rather time consuming, the availability of fast and reliable analytical prescriptions for modeling one or the other part of the full calculation is very welcome. This is most feasible for the computation of reaction and interaction cross sections. The semi-empirical parameterization by Silberberg and Tsao [14], based on the pioneering paper of Rudstam [15], is often used in this context. This prescription, more than 30 years old, was revised over the years as new measurements became available. Based on their data on spallation of iron, Webber *et al.* [16] developed another parametric formulation, which was estimated to be valid for up to medium-mass reaction partners. The recent prescription by Waddington *et al.* [17] consists of formulas for charge-changing cross sections, but no prediction is made for the product-residue mass.

Updates of former prescriptions and new developments in spallation production cross-section calculations generally depended on the particular application [18,19]. The influence of the collision energy and of the mass of the nucleus interacting with the light particle (hereafter referred to as the *reaction partner*) have to be properly accounted for. Several assumptions regarding these dependences were proposed. In the framework of so-called "limiting fragmentation" [20], the shape of the residue-mass distribution becomes independent of bombarding energy beyond a given energy. Scaling and factorization laws [20–22] were also proposed, relating the production cross section in nucleon-induced spallation to that measured in heavy-ion fragmentation by applying geometrical factors. All these hypotheses could only be partly assessed so far, and their validity was found to be system dependent. A limiting-fragmentation-like regime in spallation was not established yet [20,23], and doubts were placed on the accuracy of simple scaling relationships as well [20,16,24]. An attempt was recently [25] made to extend the well-known semi-empirical parameterization of fragmentation cross sections EPAX by Sümmerer and Blank [26] to spallation, motivated

[1]In the present paper, *fragmentation* refers to the interaction between two heavy ions (nucleus-nucleus collision), whereas *spallation* is used for the interaction between a light particle and a heavy nucleus (nucleon-nucleus collision, presently).

by the success of EPAX for heavy-ion fragmentation. Along that work, it was remarked that the mass-yield curve of the spallation residues substantially varies with energy. As a nucleon deposits less energy than a heavy ion with the same energy per nucleon does, faster nucleon projectiles are required to reach a potentially universal mass-yield profile in spallation as compared to fragmentation. Since EPAX is an energy-independent prescription, well suited in the limiting-fragmentation regime accessible with heavy-ion beams at current facilities, the attempt of extending it to spallation was not developed further in Ref. [25]. Rather, it was chosen to concentrate on improving upon the version 2 of the EPAX prescription (hereafter EPAX2) for fragmentation with the updated version 3 [27] (hereafter EPAX3). Recently, a modified parameterization of EPAX2 was proposed by Zhang [28] with the inclusion of an energy dependence, improving the predictions at intermediate energies outside the limiting-fragmentation regime. This development, based on a local fit of specific fragmentation data, does unfortunately not make EPAX more suitable for spallation reactions.

As obvious from above, a global parameterization for spallation is lacking, and different formulas are used, depending on reaction-partner mass and proton-neutron asymmetry (N/Z hereafter), bombarding energy, and product size [14]. The capability of existing prescriptions to predict cross sections with high accuracy and over a wide range remains limited, see, e.g., discussion in Refs. [29,30]. At the same time, the magnitude of current uncertainties needs to be reduced for a number of applications, see, e.g., Refs. [4,25,7,31]. In astrophysics, for example, none of the existing prescriptions meets the 10% accuracy that is desired in propagation calculations. Using the available parameterizations outside of their range of adjustment is therefore hazardous, and there is a need for a new, possibly more universal, prescription.

It is the aim of the present paper to take a step in this direction and propose a realistic parameterization of the residue isotopic production cross section in proton- and neutron-induced spallation over a large domain of reaction-partner mass, N/Z, and bombarding energy. As originally proposed by Rudstam [15], the formalism consists of two main parts, *viz.* the mass and the isobaric distribution, respectively. A new prescription of the mass yields, well suited for spallation, and explicitly accounting for the dependence on bombarding energy, is developed. The parameterization of the isobaric distribution is, on the contrary, inspired from the analytical expressions derived for the description of fragmentation reactions in EPAX [26,27]: Starting from the updated EPAX3 [27], modifications are introduced to adapt the isobaric functional prescription suited for fragmentation to the specificities of spallation. The modeling is further developed to account analytically for shell effects and even-odd staggering in the product yield as originating from the last deexcitation step of the primary fragments. The progressive washing of structural staggering caused by the competition with γ-ray emission in the decay cascade [32,33] on one side and by angular momentum effects [34] on the other side is parameterized as well. Since this structural staggering and fading out with γ-decay competition and angular momentum are independent of the reaction mechanism, the proposed formalism can be implemented in fragmentation models, too. Finally, the description of the products formed in charge-pickup processes is included also. The new parameterization is named SPACS for spallation cross sections. According to the charge independence of the reaction mechanism in the energy domain considered in this paper, it is usable for neutron- and proton-induced spallation. This paper focuses on proton-induced reactions as systematic data on isotopic yield for reactions with neutrons are scarce. Like EPAX for fragmentation, SPACS restricts to the description of the production cross section of residues down to about half of the reaction-partner mass for heavy systems and somehow below for lighter ones. This restriction is imposed by the possible contribution of fission, binary decay with intermediate-mass-fragment emission, multifragmentation, or vaporization, which populate the lower masses. Work aiming to account for the latter channels is in progress.

The paper is organized as follows. Section II is dedicated to the description of the SPACS formalism: After a short reminder on the basic features, which are identical to those used in previous parameterizations, the ideas specifically developed in this paper for the case of nucleon-induced spallation and the corresponding equations are detailed. Special attention is paid to the dependence on collision energy and to the analytical modeling of shell structure and even-odd staggering. Section III demonstrates the achievement of the new parameterization based on extensive comparison with experimental data accumulated over the last three decades from a broad variety of reactions and techniques [35]. Conclusions and perspectives are given in Sec. IV.

II. THE SPALLATION CROSS-SECTION FORMALISM

Reactions between a high-energy nucleon and a heavy nucleus can be very schematically viewed as a two-step process [36]. In the first (sometimes referred to as *fast*) stage, the incident particle penetrates the heavy nucleus and initiates a cascade of nucleon-nucleon collisions [11]. Some of the struck nucleons can escape. The avalanche of collisions in the bulk volume heats the system, and an excited thermalized nucleus, often referred to as the *prefragment*, is formed. In the second (sometimes referred to as *slow*) stage, the excited primary product cools down by particle evaporation, emission of clusters, binary decay of various types (including fission), multifragmentation, or even vaporization, depending on its initial excitation energy, angular momentum, and fissility. Emission of γ rays usually takes place at the very end of the deexcitation cascade. It has been realized long ago now that preequilibrium phenomena can take place before the evaporation-fission competition [37]. These may be handled within the modeling of the intranuclear cascade. Nonetheless, in many cases, the latter is stopped before equilibrium is reached, and a specific model for preequilibrium emission is introduced between the intranuclear cascade and the evaporation-fission competition. At present, most of the available models assume such a sequence of processes for describing the outcome of a spallation reaction (see, e.g., Refs. [38,39]). For energies well above the Coulomb barrier as considered here, capture of the incident nucleon is a weak channel. In addition, the first stage does not depend on whether the incident nucleon is a proton or

a neutron due to charge independence of nuclear forces. The subsequent stages, i.e., preequilibrium and evaporation-fission competition, are obviously independent of the charge of the incoming particle. Hence, for energies above the Fermi regime (∼50MeV/nucleon), the same formulas apply for the proton and the neutron probes [36,40].

The approach adopted in the present paper for constructing an analytical prescription of the residue production by spallation is semi-empirical, guided by the shape of measured mass and isobaric distributions, combined wherever possible, with physics arguments. Phenomenology and experimental observations are further used to adjust the parameters of the model. It may be worth noting here that, by construction, there is no explicit sequencing of the reaction into stages; the outcome of the collision is parameterized as a whole. The SPACS parameterization may be considered in the domain of spallation as the counterpart of EPAX for fragmentation. It is nonetheless emphasized that, as compared to EPAX, an additional account is made in SPACS for the dependence on collision energy as well as for shell-structure and even-odd effects.

A. Basic ideas

The gross features of spallation and fragmentation yields in the product mass and nuclear charge (A,Z) plane are qualitatively similar [25]. The integral mass distribution resembles two joined hyperbolas with the falling off occurring on the smallest mass side and an uprising tail in the opposite region close to the mass of the reaction partner. Isotopic distributions exhibit bell-like shapes, except in the region close to the reaction partner. According to these similarities, the seminal paper of Rudstam [15] established that the cross section of a final product with mass number A and nuclear charge Z for both spallation and fragmentation can be factorized as follows:

$$\sigma(A,Z) = \sigma_R Y(A) Y(Z_{\rm prob} - Z)|_A. \qquad (1)$$

The term $Y(A)$ in Eq. (1) corresponds to the mass yield (summed over all Z's), and $Y(Z_{\rm prob} - Z)|_A$ describes the isobaric element yield for a given A. The most probable charge for this particular mass is denoted by $Z_{\rm prob}$. Normalization is performed on the total reaction cross section σ_R. Equation (1) was successfully applied for spallation first by Silberberg and Tsao [14] and for fragmentation by Sümmerer *et al.* [41] and Sümmerer and Blank [26]. We follow the same overall architecture in SPACS with the main features as follows.

Despite the aforementioned qualitative similarities, a detailed survey reveals that the product mass distributions $Y(A)$ in fragmentation and spallation cannot be described with the same mathematical expression [25]. Contrary to fragmentation [26,27], the energy dependence of $Y(A)$ cannot be overlooked in spallation. As mentioned previously, to make the spallation-residue distribution extending down to the lightest masses and reach a universal (energy-independent) profile, the bombarding energy has to be particularly high in light-particle-induced reactions. No evidence for a limiting-fragmentation-like regime was established so far. Furthermore, spallation is not a process of such "clean geometrical" character: Unlike in the abrasion picture of fragmentation, in spallation there is a less well-defined region of the heavy reaction partner that is affected by the cascade shower initiated by the incident particle. That will make the dependence of the (A,Z) production on the bombarding energy rather complex. Since a global formalism is still missing for $Y(A)$ in spallation, a new parameterization is derived in the present paper, including the dependence on bombarding energy.

The deexcitation of the excited prefragment is governed by statistical processes [42], and similar analytical expressions can be adopted for the charge-dispersion curve $Y(Z_{\rm prob} - Z)|_A$ in fragmentation and spallation. The formulation of the charge dispersion retained for SPACS is thus based on the prescription successfully used in EPAX [26,27] with suited modifications specific to the case of spallation.

Structural effects are further introduced. The influence of closed shells and the even-odd staggering which were evidenced experimentally to modulate the yield of the residues (see Ref. [43] and references therein) is parameterized in a new way. Its fading out due to competition of particle evaporation with emission of γ rays as well as due to the influence of angular momentum is included also. These aspects go beyond most previous empirical analytical models. It is emphasized that they are independent of the reaction mechanism. The way in which they are parameterized in SPACS is rather general, and it can be implemented for other mechanisms in the corresponding analytical codes, too.

For the parameterization of the total spallation reaction cross section σ_R, we adopt the energy-dependent prescription developed by Tripathi and co-workers [44,45] for neutrons and protons, respectively. Some modifications were introduced as we have found it necessary to better account for the influence of the nuclear composition of the heavier reaction partner.

The above-itemized contributions to $\sigma(A,Z)$ appearing in Eq. (1) are discussed separately in the next section. Since most of the data we will consider have been collected in inverse kinematics, we identify all along this paper the heavier reaction partner with the projectile. Reference to the latter will therefore be replaced by reference to the target for analysis of direct kinematics experiments. In this context, the subscript *proj* (for projectile) in the following equations has to be substituted with *tar* (for target) in direct kinematics. We remind that the mass of the target (respectively, the projectile) is equal to 1 in inverse (direct) kinematics in the spallation reaction considered here.

B. The semi-empirical parameterization

1. Mass yield Y(A)

To derive the prescription for the mass yield, we start with a phenomenological analysis. Measured spallation-residue mass distributions suggest that $Y(A)$ can be decomposed into two contributions: A rather flat distribution with a gentle cutoff to the lower mass side and a rapid increase towards the projectile (*viz.* reaction partner) mass. We relate this observation to the interaction mechanism. The former contribution corresponds to a wide range of impact parameters where the incoming particle interacts with the nucleons of the reaction partner, whereas the latter component is due to most peripheral collisions, accounting for the density distribution and for which the number of interactions between the incoming particle and the nucleons of the reaction partner is small. It is further

assumed that the excitation energy of the prefragment mostly depends on the number of primary interactions of the incoming particle in the reaction partner so that the mass yield curve directly reflects the distribution of excitation energies in the prefragments [32]. This phenomenological analysis suggests that, for all but the largest impact parameters, the residue-mass distribution can be described with a Fermi-like function $Y(A)_{\rm cent}$, whereas peripheral collisions may be accounted for by an additional exponential-like contribution $Y(A)_{\rm periph}$. The proposed parameterization of the mass yield therefore reads

$$Y(A) = Y(A)_{\rm cent} + Y(A)_{\rm periph}, \tag{2}$$

where the central and peripheral contributions are given, respectively, by

$$Y(A)_{\rm cent} = [A_{\rm length}/(1 + \exp\{[(A_{\rm proj} - A_{\rm cent}) - A] / A_{\rm fluct}\})]/A_{\rm cent}, \tag{3}$$

and

$$Y(A)_{\rm periph} = A_{\rm periph} \exp\{[A - (A_{\rm proj} - A_{\rm diff})]/A_{\rm diff}\} \times (E_{\rm proj}/1000)^{B_{\rm periph}}/A_{\rm cent}, \tag{4}$$

with $A_{\rm proj}$ as the mass of the projectile and $E_{\rm proj}$ as its energy in MeV/nucleon. $A_{\rm length}$, $A_{\rm cent}$, $A_{\rm fluct}$, $A_{\rm periph}$, $A_{\rm diff}$, and $B_{\rm periph}$ are variables which are discussed below. Note that the mass yield is chosen to be normalized to the quantity $A_{\rm cent}$. An illustrative view of the mass yield described by Eqs. (2)–(4) is displayed in Fig. 1 for a projectile with mass 100. The profile of the curve compares well with typical experimental spallation-residue mass distributions (see Sec. III).

The precise shape of the mass-yield curve is determined by the variables entering into Eqs. (3) to (4) and their dependence on system mass and bombarding energy.

The quantity $A_{\rm cent}$ is connected to the mass removed in most central collisions according to

$$A_{\rm cent} = \alpha_{\rm cent}/\exp(A_{\rm proj}/\beta_{\rm cent}). \tag{5}$$

It increases linearly with bombarding energy as the mass removed is small compared to $A_{\rm proj}$. Since $A_{\rm cent}$ cannot exceed $A_{\rm proj}$, a saturation-like behavior with increasing bombarding energy is introduced with the ansatz,

$$A_{\rm cent} = A_{\rm proj}\{1 - \exp[-\ln(A_{\rm cent})/\ln(A_{\rm proj}) \times (E_{\rm proj}/1000)^{\varepsilon_{\rm cent}}]\}. \tag{6}$$

The term $A_{\rm length}$ is related to the nearly constant yield between $A_{\rm cent}$ and $A_{\rm proj}$. It depends on $A_{\rm cent}$, and it is affected by fluctuations $A_{\rm cent\_fluct}$ in the amount of removed mass. The following prescription is proposed:

$$\begin{aligned} &\text{for} \quad A > (A_{\rm proj} - A_{\rm cent} + \alpha_{\rm length} A_{\rm cent\_fluct}) \\ &A_{\rm length} = \sqrt{[(A_{\rm cent} + \alpha_{\rm length} A_{\rm cent\_fluct})^2 - (A_{\rm proj} + \alpha_{\rm length} A_{\rm cent\_fluct} - A_{\rm cent} - A)^2]}/(A_{\rm cent} + \alpha_{\rm length} A_{\rm cent\_fluct}), \\ &\text{for} \quad A \leqslant (A_{\rm proj} - A_{\rm cent} + \alpha_{\rm length} A_{\rm cent\_fluct}), \quad A_{\rm length} = 1. \end{aligned} \tag{7}$$

The second ansatz in Eq. (7) ensures that, for a given spallation-residue mass A, the maximum possible mass removed does not exceed $(A_{\rm proj} - A)$.

The quantity $A_{\rm cent\_fluct}$ describes the smooth fall off of the distribution due to fluctuations in the number of removed nucleons. It is parameterized as follows:

$$A_{\rm cent\_fluct} = a_{\rm fluct}(A_{\rm cent})^{\delta_{\rm fluct}}(E_{\rm proj}/1000)^{\varepsilon_{\rm fluct}}, \tag{8a}$$

where

$$a_{\rm fluct} = \alpha_{\rm fluct} + \beta_{\rm fluct} A_{\rm proj}. \tag{8b}$$

The variables $A_{\rm periph}$, $A_{\rm diff}$, and $B_{\rm periph}$, respectively, determine the magnitude, uprising slope, and height of the contribution by peripheral collisions. They are parameterized according to

$$A_{\rm periph} = \alpha_{\rm periph} + \beta_{\rm periph} A_{\rm proj}, \tag{9a}$$

$$A_{\rm diff} = \alpha_{\rm diff} + \beta_{\rm diff} A_{\rm proj}, \tag{9b}$$

$$B_{\rm periph} = \gamma_{\rm periph}[1 + \exp(-\{[\ln(1000)/\ln(E_{\rm proj})]^6 + \varepsilon_{\rm periph}\}/\delta_{\rm periph})]. \tag{9c}$$

The parameters ($\alpha_{\rm cent}$, $\varepsilon_{\rm cent}$, $\alpha_{\rm length}$, $\alpha_{\rm fluct}$, $\beta_{\rm fluct}$, $\delta_{\rm fluct}$, $\varepsilon_{\rm fluct}$, $\alpha_{\rm periph}$, $\beta_{\rm periph}$, $\alpha_{\rm diff}$, $\beta_{\rm diff}$, $\gamma_{\rm periph}$, $\varepsilon_{\rm periph}$, $\delta_{\rm periph}$) appearing in Eqs. (4)–(9) are constants (see Table I in Appendix), which were adjusted along comparison with experiment.

2. *Isobaric distribution*

Contrary to the mass yield, the isobaric (equivalently, isotopic) distributions are rather insensitive to the interaction mechanism and are primarily governed by level-density considerations [32]. The bell-shaped function reflects the profile of the so-called evaporation corridor [32,33,46,47]. As mentioned above, the prescription for the element distribution at fixed mass $Y(Z_{\rm prob} - Z)|_A$ is here borrowed from the EPAX parameterization [26] for fragmentation, including its most recent developments [27]. Accordingly, the charge dispersion in SPACS is assumed to take the form

$$Y(Z_{\rm prob} - Z)|_A = n f_{n,p} \exp(-R|Z_{\rm prob} - Z|^{U_{n,p}}). \tag{10}$$

It is characterized by three leading terms which are discussed in this section: the most probable charge $Z_{\rm prob}$ for a given mass A, and the quantities R and $U_{n,p}$ which describe the width and the shape, respectively, of the fall off of the Z distribution for a given A. The slope parameter $U_{n,p}$ takes a different value on the neutron- (U_n) and proton- (U_p) rich sides [26,27], i.e., the isobaric distribution centered around $Z_{\rm prob}$ and with a width R, is not symmetrically parameterized

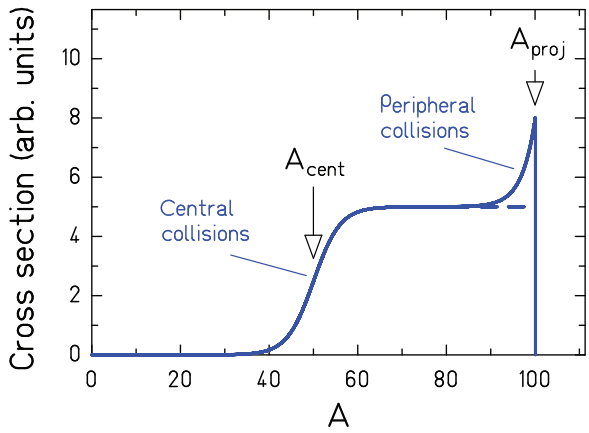

FIG. 1. (Color online) Schematic behind the functional form used to parameterize the mass yield $Y(A)$ in SPACS. See the text for the signification of the indicated quantities.

in accordance with experimental observation. The factor $n = \sqrt{(R/\pi)}$ normalizes the integral of the charge dispersion curve to unity, whereas $f_{n,p}$ is a correction factor specific to neutron- and proton-rich products, respectively. We found it necessary to adjust some formulas of EPAX3 [27] to match the specificities of spallation. These modifications, detailed below, were guided by experimental observation.

The most probable charge $Z_{\rm prob}$ for a given mass (maximum of the isobaric distribution) is parameterized relative to the valley of β stability as in Refs. [26,27],

$$Z_{\rm prob} = Z_\beta + \Delta + \Delta_m^{n,p} + 0.002A. \tag{11}$$

For projectiles not too far from stability, $Z_{\rm prob}$ deviates from Z_β by the quantity Δ so that $Z_\beta + \Delta$ defines the attractive evaporation corridor. The quantity $\Delta_m^{n,p}$ accounts for the "memory effect" of the neutron or proton excess of the projectile, whereas the last term in Eq. (11) is a small empirical offset introduced in Ref. [27].

In Ref. [25] the value of Δ for the deviation of $Z_{\rm prob}$ from stability was examined using experimental data on spallation of iron and lead over a wide range of product mass A. From the compilation reported in Fig. 1 of Ref. [25] (top right panel), the dependence of the parameter Δ on A is observed to be slightly different in spallation and in heavy-ion fragmentation. The centroid of the isobaric distribution is located more towards the neutron-deficient side in spallation. This indicates that more excitation energy has to be deposited in the prefragment to reach a certain product mass as compared to fragmentation [48]. On the basis of this observation, we keep the main functional form, but we add higher-order terms and change the value of some of the parameters entering the definition of Δ as compared to EPAX. This yields

$$\begin{aligned} &\text{for} \quad A \geqslant \Delta_6, \quad \Delta = \Delta_1 + \Delta_2 A + \Delta_3 A^2 + \Delta_4 A^3, \\ &\text{for} \quad A < \Delta_6, \quad \Delta = \Delta_5 A^2. \end{aligned} \tag{12}$$

To improve further the description of spallation data, additional corrections have been brought to Eq. (12) depending on the distance of the product from the projectile, according to

$$\begin{aligned} &\text{for} \quad A/A_{\rm proj} > d_2 \quad \text{and} \quad A/A_{\rm proj} \leqslant d_3, \\ &\qquad \Delta = \Delta[1 + d_1(A/A_{\rm proj} - d_2)^2], \end{aligned} \tag{13}$$

$$\begin{aligned} &\text{for} \quad A/A_{\rm proj} > d_2, \\ &\qquad \Delta = \Delta[1 + d_1(A/A_{\rm proj} - d_3)^3]. \end{aligned} \tag{14}$$

Since spallation implies higher prefragment excitation energy for a given product mass than fragmentation does, we need to readjust the parameter Δ_m too. Starting from the prescription derived in Refs. [26,27], best agreement with experiment is obtained for spallation after slight modification of the functional form for neutron-rich projectiles and introducing additional terms for proton-rich ones:

$$\text{for} \quad (Z_{\rm proj} - Z_{bp}) \leqslant 0 \text{ (neutron-rich projectile)},$$

$$\Delta_m^n = \{n_1(A/A_{\rm proj})^6 + n_2[(A_{\rm proj} - A)/A_{\rm proj}]^2\} \times (Z_{\rm proj} - Z_{\beta p}), \tag{15a}$$

$$\text{for} \quad (Z_{\rm proj} - Z_{bp}) > 0 \text{ (proton-rich projectile)},$$

$$\Delta_m^p = [\exp(p_1 + p_2\, A/A_{\rm proj})](Z_{\rm proj} - Z_{\beta p}), \tag{15b}$$

supplemented with

$$\Delta_m^p = \Delta_m + p_3[(A_{\rm proj} - A)/A_{\rm proj}]^2 \times (Z_{\rm proj} - Z_{\beta p}) \quad \text{for} \quad A/A_{\rm proj} < 0.5, \tag{15c}$$

$$\Delta_m^p = \Delta_m + \{\exp[-(d_3 - A/A_{\rm proj})^2/0.005]\} \times (Z_{\rm proj} - Z_{\beta p}) \quad \text{for} \quad A \geqslant \Delta_6. \tag{15d}$$

The width parameter[2] R of EPAX [26,27] depends at first order on the product mass,

$$R = r_0 \exp(R_1 A + R_2 A^2). \tag{16}$$

According to Eq. (16), far enough from the projectile, the width of the isobaric distribution decreases with decreasing A. It remains finite at $A = 0$ for which it is equal to the constant r_0. We propose reexamining the derivation of the R parameter in this paper, based on a few more physics ideas.

At first approximation, due to the symmetry energy proportional to $(N - Z)$ in a liquid-drop picture, the nuclide distribution is compressed towards the evaporation corridor [47,49]. The width of the distribution should therefore go to zero for $A \to 0$ (equivalently, R should tend to infinity). Nevertheless, despite this strong "restoring force," the distribution keeps a minimum width in $(N - Z)$ at fixed mass due to the fluctuations induced by evaporation [32]: Evaporation of one proton or one neutron inevitably changes the $(N - Z)$ of the product by a finite amount, causing a statistical fluctuation and hence a minimum width in $(N - Z)$, even for the lightest residues. We revisit Eq. (16) based on these two ideas.

[2]The parameter R is related to the variance σ^2 of the isobaric distribution according to $R = 1/(2\sigma^2)$.

To obey the restoring force, we start with the following prescription $R^{\rm phy}$ within which the isobaric distribution width tends to zero for $A \to 0$:

$$\text{for} \quad A < t_1, \quad R^{\rm phy} = R_0^{n,p} \exp\{-\ln[R_1(A/t_2)]\}, \tag{17a}$$

$$\text{for} \quad A \geqslant t_1, \quad R^{\rm phy} = R_0^{n,p} \exp(R_2 + R_3 A + R_4 A^2), \tag{17b}$$

where t_1 and t_2 are constant parameters.

As proposed in EPAX3 [27], we adopt a dependence of the variable $R_0^{n,p}$ on the projectile. This was motivated by the observation that experimental isobaric distributions are a bit wider for neutron-rich projectiles. We adapted the formulas of Ref. [27] to spallation and obtained

$$\text{for} \quad (Z_{\rm proj} - Z_{\beta p}) \leqslant 0 \text{ (neutron-rich projectile)},$$

$$R_0^n = r_0 \exp[r_3(Z_{\rm proj} - Z_{\beta p})], \tag{18a}$$

$$\text{for} \quad (Z_{\rm proj} - Z_{\beta p}) > 0 \text{ (proton-rich projectile)},$$

$$R_0^p = r_0 \exp[r_4(Z_{\rm proj} - Z_{\beta p})]. \tag{18b}$$

Contrary to the prescription for fragmentation [26,27] where the R_i's (i = 2–4) Eq. (17) are assumed constant, in SPACS these variables are chosen to depend explicitly on the distance of the projectile from β stability according to

$$R_i = r_{i,0} + r_{i,1}|Z_{\rm proj} - Z_{\beta p}|. \tag{19}$$

Fluctuations caused by evaporation are additionally introduced as follows: Although a minimum width in $(N - Z)$ has been quantified in Ref. [32], we treat the fluctuation $\sigma_{\rm fluct}$ in the isobaric width as a free parameter. Adding the contributions to the variance quadratically yields a new parameter R to be inserted in Eq. (10) in replacement of Eq. (16) for light products and not too close from the projectile,

$$R = 1/\left\{2\left[1/(2R^{\rm phy}) + \sigma_{\rm fluct}^2\right]\right\} \quad \text{for} \quad A < t_1 \text{ and } A/A_{\rm proj} < r_2,$$
$$R = R^{\rm phy}, \text{ otherwise.} \tag{20}$$

The additional correction introduced in Ref. [27] close to the projectile is adopted after slight adjustment to spallation for which we observed a stiffer slope of the isotopic distribution close to the projectile as compared to fragmentation,

$$R' = R \exp[r_1 \sqrt{A_{\rm proj}(A/A_{\rm proj} - r_2)^5}] \quad \text{for} \quad A/A_{\rm proj} \geqslant r_2. \tag{21}$$

We emphasize that the ideas behind the new prescription for the width parameter R Eqs. (17) and (20) hold for spallation *and* fragmentation. That is, these equations may be useful to be implemented in analytical models of fragmentation, such as EPAX. The modification affects the description of the lighter-mass products, leading to narrower isobaric distributions than Eq. (16) would do, and in better agreement with experiment. For systems of astrophysical and medical interests, a reduction in the isobaric width of up to (20–30)% is estimated when replacing Eq. (16) with Eqs. (17) and (20). That can impact substantially predictions for most exotic isotopes.

The experimentally observed non-Gaussian fall off of the isobaric distribution is modeled with the exponents U^n and U^p, which expressions we found necessary to slightly modify for spallation as compared to Refs. [26,27], according to

$$U^n = u_{n_1} + u_{n_2} A/A_{\rm proj}, \tag{22}$$

$$U^p = u_{p_1} + u_{p_2} A_{\rm proj}. \tag{23}$$

Normalization of the charge-dispersion curve is further refined as proposed in EPAX3 [27] by additional correction factors $f_{n,p}$ for neutron- and proton-rich products, respectively. A so-called "brute-force factor" f_n [27] was found necessary for very neutron-rich fragments where

$$f_n = 10^{[-b_1|Z_{\rm proj} - Z_{\beta p}|(Z_\beta - Z + Z_{\rm proj} - Z_{\beta p} + b_2)^3]} \quad \text{for} \quad (Z_\beta - Z) > (Z_{\rm proj} - Z_{\beta p} + b_2),$$
$$f_n = 1, \text{ otherwise.} \tag{24}$$

For very proton-rich fragments, the mandatory correction factor was parameterized [26,27] with

$$f_p = 1/[10(dF/dZ)^{(Z - Z_{\rm exp})}] \quad \text{for} \quad Z > Z_{\rm exp}, \tag{25}$$

where $dF/dZ = 1.2 + 0.647(A/2)^{0.3}$ and $Z_{\rm exp} = Z_{\rm prob} + dF/dZ \ln(10)/(2R)$.

Finally, the SPACS formalism is extended to the description of charge-exchange channels ($Z > Z_{\rm proj}$). This channel is not considered in EPAX. Modeling of charge pickup is achieved by applying to the charge-dispersion curve formula for $Z > Z_{\rm proj}$ a factor f_{pu} which reads

$$f_{pu} = a_{pu} + b_{pu} \exp[-(E_{\rm proj}/1000)/c_{pu}] \quad \text{for} \quad E_{\rm proj} < 1000\,\text{MeV/nucleon},$$
$$f_{pu} = 1 \quad \text{for} \quad E_{\rm proj} \geqslant 1000\,\text{MeV/nucleon}. \tag{26}$$

The energy dependence of charge exchange was parameterized using the experimental data measured in Ref. [50] and normalized to its value at 1000 MeV/nucleon in Eq. (26).

3. *Structural and even-odd staggering, competition by γ-ray emission and angular-momentum effects*

a. Influence of nuclear shells, and pairing correlations. The pattern of the production cross sections of the light residues has been observed in several kinds of reactions to be characterized by a strong staggering, reflecting the influence of both shell effects and pairing correlations (see Refs. [43,49,51–57] and references therein). Although of weaker magnitude, a similar staggering was observed in heavy products close to the projectile [58,59]. In the SPACS parameterization, we follow the suggestion of Ref. [49] where staggering in the production cross section is explained by the influence of nuclear separation energies on the evaporation process. This explanation is based on an idea originally formulated by Hüfner *et al.* [60], and according to which the cross section of a specific residue is proportional to its lowest particle threshold. The latter is directly related to shell structure and pairing correlation in nuclei [61]. The idea of Ref. [60] can be understood in the following way: We may assume that the primary production of the nuclear reaction, before the evaporation cascade, is structureless in Z, A, and excitation energy. Most part of the excitation energy is located above the corresponding lowest particle threshold. This three-dimensional cloud is transported by evaporation of neutrons, protons, and other light-charged particles to the respective daughter nuclei with excitation energies that are essentially reduced by the corresponding "effective" particle thresholds.[3] At this stage, it should be mentioned that Monte Carlo event generators, as they explicitly compute the evaporation sequence, automatically take the influence of shell structure and pairing in binding energies into account. Hence, they are naturally suited to address the observed even-odd staggering, and they perform well (see, e.g., Refs. [38,43,62]). To account for it in a phenomenological parameterization of the entire history of the reaction, an analytical formulation has to be derived. To do so in SPACS, we start from the idea of Ref. [60]. According to this picture, the contribution of a specific primary fragment to the cross section of a specific final product by neutron evaporation is given by the primary production in an energy range between $E^*_{\rm primary} = 0 + S_n(A_{\rm final}+1,Z) + S_n(A_{\rm final}+2,Z) + \cdots + S_n(A_{\rm primary}-1,Z) + S_n(A_{\rm primary},Z)$ and $E^*_{\rm primary} = S_{\rm lpet}(A_{\rm final},Z) + S_n(A_{\rm final}+1,Z) + \cdots + S_n(A_{\rm primary}-1,Z) + S_n(A_{\rm primary},Z)$, where $S_n(A,Z)$ is the effective neutron separation energy of a nucleus of mass A and atomic charge Z and $S_{\rm lpet}(A,Z)$ is the lowest particle energy threshold of that nucleus. Similar equations are valid for any evaporation path consisting of the mixed evaporation of protons, α and other charged particles (Z will be changed accordingly in the brackets). In all these equations, the width of the energy range that ends up in a specific final fragment is given by $S_{\rm lpet}(A_{\rm final},Z_{\rm final})$. Since the lowest particle energy threshold is affected by structural effects due to nuclear shells and pairing, one expects that the same structure is found in the production cross sections.

[3]The effective particle threshold is the sum of the particle threshold and the average kinetic energy of the evaporated particle. Fluctuation in the particle kinetic energy is neglected because it is small compared to the separation energy.

To account for these ideas, we modulate the (smooth) distribution derived in Sec. II B 2 by a staggering caused by shell and even-odd effects. Technically, this is performed by correcting the isotopic yield $Y(A, Z)$ of Eq. (10) with the so-called structure factor $F_{e\text{-}o}(A, Z)$. For a given (A, Z) final product, this factor is determined by the ratio,

$$F_{e\text{-}o}(A,Z) = S_{\rm lpet}(A,Z)^{\rm EMP} / S_{\rm lpet}(A,Z)^{\rm MAC}, \qquad (27)$$

where $S_{\rm lpet}(A,Z)^{\rm EMP}$ and $S_{\rm lpet}(A,Z)^{\rm MAC}$, respectively, are the empirical and macroscopic lowest particle energy thresholds of the product (A, Z). Since the latter threshold, as computed with a macroscopic model, does not account for microscopic effects, the ratio Eq. (27) is a measure of the shape and magnitude of the modulation by structural effects of the smooth (macroscopic) trend.

The empirical lowest particle energy threshold is determined from most recent experimental separation energies [63]. In case of unavailable experimental masses, the Thomas-Fermi predictions of Myers and Swiatecki [64] are used for determining $S_{\rm lpet}(A, Z)^{\rm EMP}$. The macroscopic lowest particle energy thresholds $S_{\rm lpet}(A, Z)^{\rm MAC}$ are obtained from the Thomas-Fermi masses [64] without shell effects and pairing correlations. Empirical and macroscopic separation energies are beforehand corrected by the Coulomb barrier B wherever suited. In the present model, $S_{\rm lpet}(A, Z)$ is computed from the comparison of one neutron, proton, and α-particle separation energies. Restriction to those particles is reasonable for the present purpose related to the last steps of the heavy-spallation product decay. In the rare cases where experiment and theory yield a different type of particle having the lowest binding energy, the experimental (or empirical) result ultimately defines the less bound particle to be used in Eq. (27). We restrict to ground-state-to-ground-state decays and neglect the influence of possible isomers. The effect of this restriction is negligible for the present purpose. Yet, for specific interest, the influence of isomers has to be checked, and pertinent isomeric state have to be accounted for in the computation of the separation energies [65]. To avoid numerical problems near the drip lines where $F_{e\text{-}o}(A, Z)$ can become very large, the magnitude of the structure factor is limited to $F_{e\text{-}o}(A,Z) \leqslant 2$.

The above-outlined simple model must be refined to account for the reduction of staggering due to two effects [43], which are as follows: (i) the competition between particle evaporation and γ-ray emission and (ii) the influence of angular momentum. The prescriptions used to parameterize these two aspects are presented separately below. The attenuation is assumed to be of the same form for shell and pairing effects.

b. Competition by γ-ray emission. In general, above the particle threshold, the emission of γ rays is much less probable than decay by particle evaporation. According to the increase of the level density with mass, the width for decay between the ground state and the particle threshold of a given heavy nucleus can nonetheless be comparable to the decay width to the daughter residue after particle evaporation at energies close to the particle threshold. Cooling by emission of a γ ray or by a light particle thus become competitive channels. The former decay implies the survival of the initial nucleus. As discussed in detail in Refs. [43,49], competition with emission of a γ ray leads to fading out of structural effects. The magnitude

of the attenuation depends on the probability of γ decay near the particle threshold. Restricting to evaporation of neutrons, protons, and α particles in competition with γ rays, this probability reads

$$P_\gamma = \Gamma_\gamma/(\Gamma_n + \Gamma_p + \Gamma_\alpha + \Gamma_\gamma), \tag{28}$$

where $\Gamma_{n,p,\alpha,\gamma}$ are the decay widths of the corresponding channel. The radiative decay width (in MeV) around the particle separation energy is calculated following Ignatyuk [66]:

$$\Gamma_\gamma = 0.624 \times 10^{-9} A^{1.6} T^5, \tag{29}$$

where the temperature of the nucleus with mass A at low excitation energy is reasonably approximated with $T = A^{-2/3}/(0.057 + 0.00193\ \delta U)$ [67] with δU being the ground-state shell effects from Ref. [64]. Neutron Γ_n, proton Γ_p, and α particle Γ_α decay widths are parameterized reckoning the geometrical cross section and level density of the emitter according to

$$\Gamma_n = C_n(A-1)^{2/3} T/[1/T\ \exp(S_n/T)], \tag{30a}$$

$$\Gamma_{p,\alpha} = C_p(A-1,4)^{2/3}\,[2T^2/(2T + B_{p,\alpha})]/ \times [1/T\ \exp(S_{p,\alpha} + B_{p,\alpha})/T], \tag{30b}$$

where $C_{n,p,\alpha}$ are numerical factors which were adjusted by considering the magnitude of even-odd effects in low-energy fission and by model calculations, respectively. $B_{p,\alpha}$ is the proton and α-particle Coulomb barrier.

The reduction in shell structure and even-odd staggering caused by competition of γ-ray emission is finally introduced in SPACS by convoluting the structural factor of Eq. (27) with a smoothly increasing function of the spallation-product mass number as follows:

$$F^\gamma_{e\text{-}o}(A,Z) = \exp\{\ln[F_{e\text{-}o}(A,Z)](1 - C_\gamma P_\gamma)\}, \tag{31}$$

with C_γ as a parameter determining the strength of γ-ray competition and which was adjusted in comparison with experiment.

c. Influence of angular momentum. As the demonstration by Moretto [34] shows, the magnitude of pairing correlations is weakened by nuclear rotation. To estimate the angular momentum imparted to a given fragment (A, Z) in the spallation process, we use the analytical formalism derived in Ref. [68] based on shell-model considerations. The spin-cutoff parameter is expressed as a function of the difference in mass between the projectile and the final fragment only,

$$\sigma^2 = 0.16A^{2/3}(A_{\rm proj} - A)\,(2A_{\rm proj} + A)/[9(A_{\rm proj} + 1)]. \tag{32}$$

The average angular momentum of the fragment follows from $J = (\sqrt{\sigma^2} - 0.5)$.

Fading out of shell effects and even-odd staggering caused by rotation is introduced in SPACS, similar to γ competition. The structural factor of Eq. (31) is further attenuated with a smoothly increasing function of the spallation-product average angular momentum according to

$$F^{\gamma,L}_{e\text{-}o}(A,Z) = F^\gamma_{e\text{-}o}\,(A,Z)/[1 + (J - J_{cr})/D], \tag{33}$$

where J_{cr} and D are parameters that were adjusted along comparison with experiment.

As will be observed in Sec. III, shell and even-odd effects are most visible in spallation of rather light nuclei (iron and below). For spallation of medium-mass systems (e.g., xenon), a staggering is observed close to the projectile, although weaker in magnitude due to the onset of competition by γ decay. When going away from the projectile, this staggering progressively vanishes due to the additional influence of the angular momentum which increases with mass loss. For spallation of heavy nuclei (e.g., lead), apart from a weak effect close to the projectile, even-odd staggering is hardly discernible, according to the strong γ-decay probability and angular momentum effects. The selective dependence of structural staggering and its fading out on the projectile mass on one side and the product mass on the other side combined with the availability of a widespread set of experimental data, permits adjusting separately the parameters entering Eqs. (27)–(33).

We emphasize that, according to the independence of structural and even-odd effects on the reaction mechanism (see literature quoted above and in Ref. [43]), the formalism developed in this paper can be applied to other processes and, namely, to fragmentation. Equations (27)–(33) can be transported to the corresponding analytical models without change, apart from a possible re-adjustment of specific parameters. In particular, the values of J_{cr} and D have to be checked due to the expected difference in the angular momentum induced in heavy-ion fragmentation and nucleon-induced spallation [11,69].

4. Total reaction cross section

The mass yield folded by the charge distribution of Eq. (1) is finally normalized to the total reaction cross section. In SPACS the normalization is based on the prescription developed by Tripathi *et al.* for reactions induced by protons [45] and neutrons [44], respectively. In both cases, the total reaction

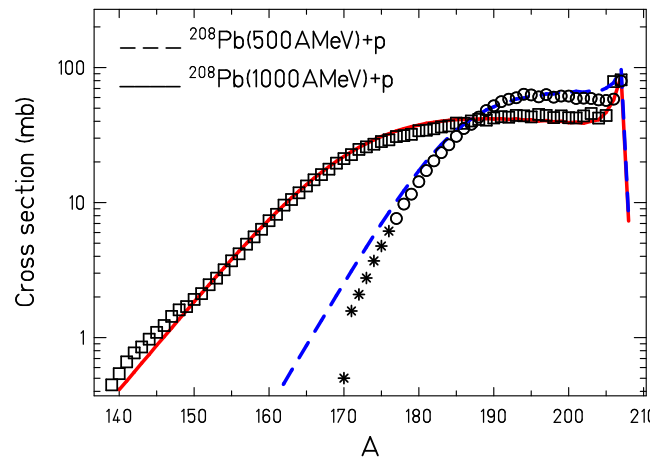

FIG. 2. (Color online) Mass distributions of the residues produced in the reactions induced by ^{208}Pb projectiles on a hydrogen target at 500-MeV/nucleon [74] (circles and stars) and 1000-MeV/nucleon [70] (squares) beam energy. The 500-MeV/nucleon data with $A < 176$ (stars) are incomplete and represent lower limits only. The measurements are compared to the predictions by the SPACS code (dashed blue and full red lines at 500 and 1000 MeV/nucleon, respectively). Not to overload the figure, experimental error bars (below 10% in most cases) are not shown.

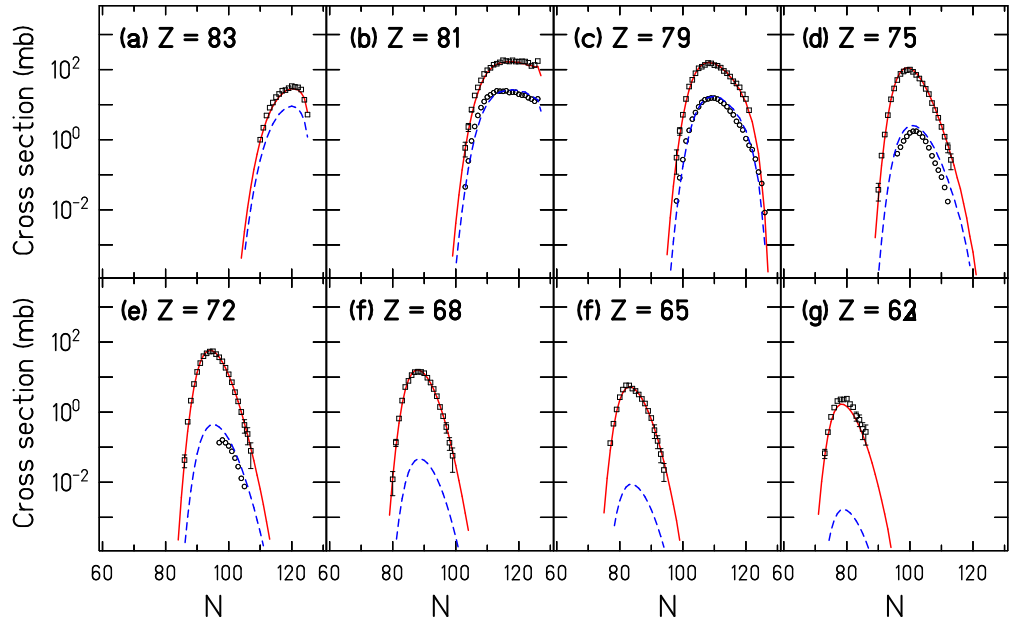

FIG. 3. (Color online) Sample of experimental isotopic distributions of the residues produced in the reactions induced by ^{208}Pb projectiles on a hydrogen target at 500-MeV/nucleon [74] (circles) and 1000-MeV/nucleon [50,70] (squares) beam energy. For clarity, the data at 1000 MeV/nucleon have been scaled by a factor of 10. The isotopic distributions of elements below $Z = 69$ and in the charge-pickup channel ($Z = 83$) are not available yet for the 500-MeV/nucleon run. Wherever not visible, experimental error bars are smaller than the symbols. The measurements are compared to the predictions by SPACS (dashed blue and full red lines at 500 and 1000 MeV/nucleon, respectively).

cross section is parameterized as follows:

$$\sigma_R\,(\text{mbarn}) = 10\pi r_0^2\left(A_{\text{proj}}^{1/3} + A_{\text{tar}}^{1/3} + \delta_E\right)^2(1 - B/E_{CM})\chi_m, \tag{34}$$

where $r_0 = 1.1$ fm, E_{CM} is the energy of the colliding system in the center of mass, and B is the Coulomb barrier. The term B/E_{CM} in Eq. (34) is, of course, absent for neutron-induced spallation. The quantity δ_E is an energy-dependent function

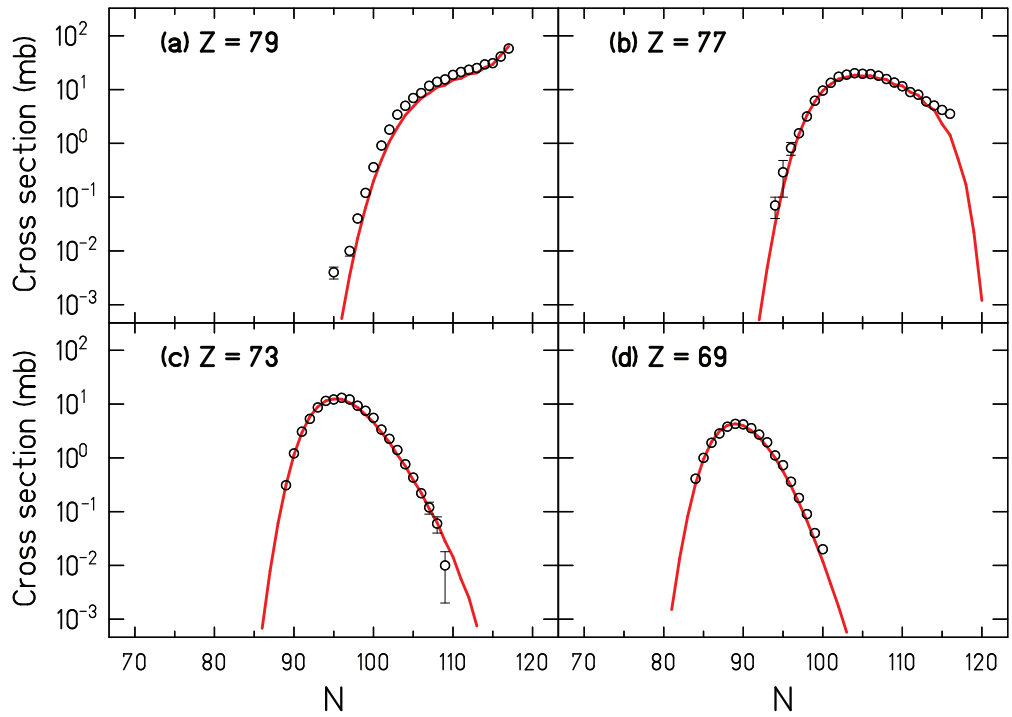

FIG. 4. (Color online) Sample of experimental isotopic distributions of the residues produced in the reactions induced by ^{197}Au projectiles on a hydrogen target at 800-MeV/nucleon beam energy [48] (circles). The measurement is compared to the predictions by SPACS (full red lines). Wherever not visible, experimental error bars are smaller than the symbols.

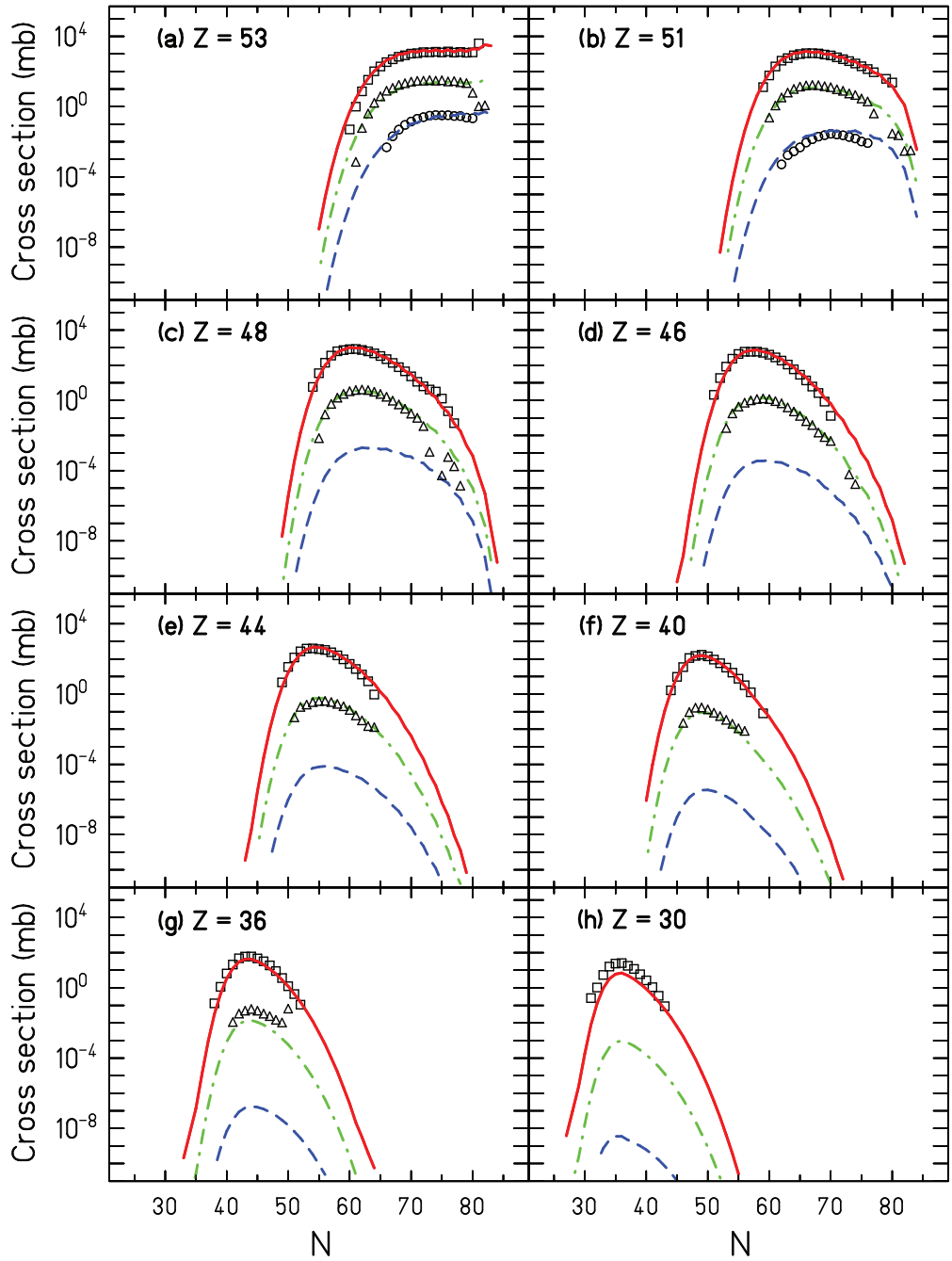

FIG. 5. (Color online) Sample of experimental isotopic distributions of the residues produced in the reactions induced by ^{136}Xe projectiles on a hydrogen target at 200-MeV/nucleon [76] (circles), 500-MeV/nucleon [60] (triangles), and 1000-MeV/nucleon [77] (squares) beam energy. Experimental error bars are, in general, smaller than the symbols and are not shown. For clarity, the data at 200 and 1000 MeV/nucleon have been scaled by factors of 10^{-2} and 10^{2}, respectively. The measurements are compared to the predictions by SPACS (dashed blue, dashed-dotted green, and full red lines at 200, 500, and 1000 MeV/nucleon, respectively). Experimental distributions are not available yet below $Z = 51$ for the 200-MeV/nucleon run.

accounting for effects of transparency and Pauli blocking, whereas χ_m corrects for the strength of the optical model interaction at low energies. The functional forms used in this paper for B, δ_E, and χ_m are borrowed from Refs. [44,45] with some modifications for δ_E and χ_m based on a better description of recent experimental data. The complete set of formulas entering Eq. (34) is given in the Appendix.

C. Summary of the SPACS package and parameters

Summing up, the SPACS parameterization comprises two classes of variables and parameters: those quantities which are specific to spallation, dealing with the modeling of the mass yield [Eqs. (1)–(9)] and the total reaction cross section [Eq. (34)] and those quantities required for modeling the charge-dispersion curve [Eqs. (10)–(26)] and the structural

staggering [Eqs. (27)–(33)] which are essentially common to spallation and fragmentation.

As detailed above, the charge-dispersion formalism is largely inspired from EPAX [26,27], whereas the total reaction cross section relies on the formulas derived by Tripathi and co-workers [44,45]. In both cases, suited modifications and adjustment of variables and parameters were introduced for either matching the specificities of spallation or improving upon the existing prescriptions. New parameterizations were developed in this paper for the spallation mass yield, for the width of the isobaric distribution, for the staggering caused by shell-structure and pairing correlations, and its fading out due to γ competition and angular momentum. We emphasize again that the development made along this work for the charge-dispersion curve on one side and the inclusion of structural effects on the other side is independent of the reaction mechanism. Corresponding equations can be implemented in other empirical models, such as, e.g., EPAX for fragmentation.

A self-sufficient summary of the SPACS formalism and the complete list of numerical values of the parameters are reported in the Appendix. Given the wide range of validity in $A_{\rm proj}$ and $E_{\rm proj}$ (from C to Bi, above about 50 MeV/nucleon), the limited number of parameters is noteworthy. Existing models make use of expressions using numerous functional forms and adjustable parameters, which both vary with system and product size (see. e.g., Refs. [14,16]). In this respect, SPACS offers a rather universal formulation.

III. RESULTS

The reliability of the predictions by the new parameterization of isotopic spallation production cross sections SPACS is studied in detail in this section. Calculations are first compared to the data collected at GSI (Sec. III A) where complete measurements have been made available recently for various systems, including light, medium-mass, and heavy nuclei over a wide energy range.[4] We further consider experiments performed at Lawrence Berkley National Laboratory (LBL), Berkeley, involving lighter systems over a comparable energy domain (Sec. III B). Both at GSI and LBL, inverse kinematics was used, and the spallation products were isotopically identified in a spectrometer. The model is next compared to excitation functions of selected residues identified by γ-ray spectrometry in direct kinematics experiments (Sec. III C). Finally, the parameterization is confronted to element yields collected at ultra-relativistic energy (Sec. III D). All these measurements permit probing in detail, over a wide range, and down to the presence of structural effects, the system-size, system-energy, and system-(N/Z) dependences as implemented in SPACS. The predictions by the code are also compared to that of other models, including intranuclear cascade simulations and commonly used empirical parameterizations (Sec. III E). As already noted, due to the paucity of corresponding data, the comparison is restricted in this paper to proton-induced reactions, but SPACS is applicable also to neutron-induced spallation.

We remind that, similar to EPAX for fragmentation, the semi-empirical parameterization for spallation SPACS is not meant to describe fission, binary decays with intermediate-mass-fragment emission, or multifragmentation and breakup processes. Its use is thus restricted to low-fissility systems, and product residues for which the contribution of the aforementioned channels is weak. For the heaviest nuclei considered in this paper, ^{208}Pb and ^{209}Bi, the fission cross section has been measured [70–72]; it is sufficiently small and far in mass for not sizably affecting the spallation-residue distribution. Binary decays with emission of intermediate-mass fragments and multi-fragmentation-like phenomena contribute for not more than a few percents at ~1000 MeV/nucleon [73]. To limit the influence of the latter at higher energy, the parameterization is recommended to be used for the description of products corresponding to a mass loss smaller than about 50% of the reaction-partner mass for heavy systems and about more for lighter systems.

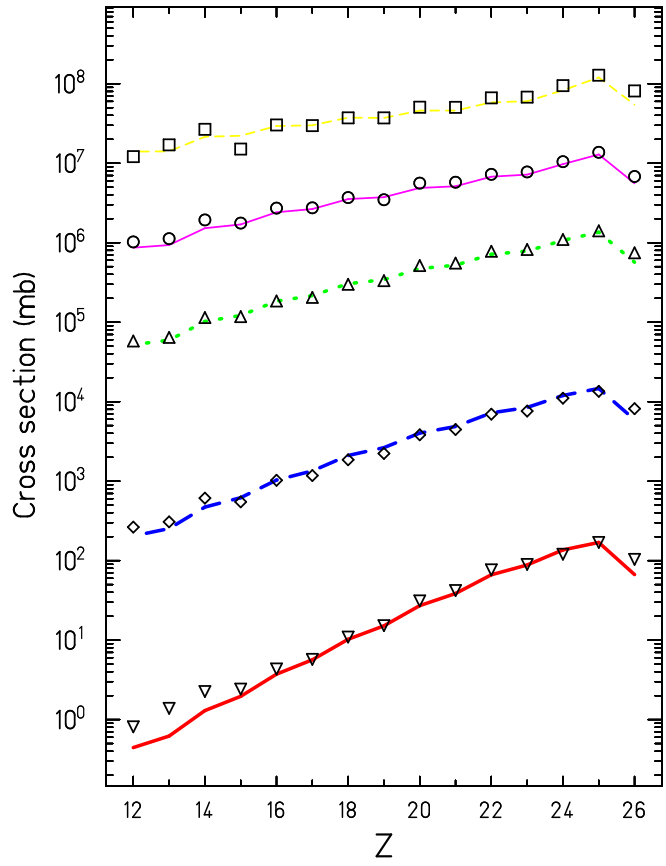

FIG. 6. (Color online) Experimental element distributions of the residues produced in the reactions induced by ^{56}Fe projectiles on a hydrogen target at 300-MeV/nucleon (downwards triangles), 500-MeV/nucleon (diamonds), 750-MeV/nucleon (upwards triangles), 1000-MeV/nucleon (circles), and 1500-MeV/nucleon (squares) beam energy [29,78]. Error bars are smaller than the symbols. For clarity, the data have been scaled by factors of 10^2, 10^4, 10^5, and 10^6 at 500, 750, 1000, and 1500 MeV/nucleon, respectively. Lines correspond to model predictions with SPACS.

[4]The comprehensive GSI data set on spallation of iron, xenon, and lead with bombarding energies from 200 to 1500 MeV/nucleon was in particular used to adjust the model parameters.

A. Comparison with GSI data: from Fe to Pb from 200 to 1500 MeV/nucleon

Experimental and calculated mass distributions are compared in Fig. 2 for the spallation residues produced in the bombardment of an hydrogen target by a ^{208}Pb beam at 500 [74] and 1000 [70] MeV/nucleon. The SPACS parameterization is observed to well reproduce the measurement. The main features of the curve (fall off close to the projectile, plateau region, and exponential decrease towards lower mass) are properly described. Also, the strong dependence on bombarding energy is reproduced. The apparent discrepancy observed for the data at 500 MeV/nucleon for A below 176 is due to the analysis of the measurement which is incomplete in this region (elements with $Z < 69$ were not analyzed). The experimental values, corresponding to lower limits, have been represented by stars in the figure. The discrepancy between the measured and the calculated slope below $A \sim 185$ for the 500 MeV/nucleon run may be ascribed to the difficult correction for secondary reactions [74]. Figure 3 further shows that SPACS describes well the residue isotopic distributions. Also, the charge-pickup channel [50] is well accounted for. The evolution of the distributions, i.e., location of the maximum, width, and skewness, when progressively going away from the projectile is properly described over the wide mass-loss range measured with cross sections spanning up to four orders of magnitude. Good agreement is obtained also (not shown) between the model calculations and the data measured by Gloris *et al.* [75] for ^{208}Pb + p between 70 and 2600 MeV/nucleon.

A nearby heavy system is considered in Fig. 4 with the reaction ^{197}Au (800 MeV/nucleon) + p [48] from the GSI campaign. As for the lead projectile, the measured isotopic distributions are well reproduced by the analytical prescription. Again, the change in shape of the isotopic distribution from close to the projectile to lighter elements is properly described.

Going down in projectile mass, we consider in Fig. 5 the system ^{136}Xe + p which was investigated at various energies [60,76,77] at GSI. For the 500 and 1000 MeV/nucleon runs, the figure illustrates the good description by the code, down to far away from the projectile. A proper description is also observed at 200 MeV/nucleon close to the projectile. The analysis of the latter data is still in progress [76] to account for the increasing influence of secondary reactions in the lighter products at this energy so that no more elements are shown. Figure 5 demonstrates the quality of the energy dependence as implemented in SPACS in describing the evolution of the shape of the isotopic distribution with bombarding energy.

The predictions by SPACS and comparison with experiment for the lightest system measured at GSI are presented in Figs. 6 and 7 with the reaction ^{56}Fe + p at 300, 500, 750, 1000, and 1500 MeV/nucleon bombarding energy [29,78]. Integral element distributions are shown for all energies in Fig. 6, whereas isotopic distributions, from very close (Z = 26) to quite far (Z = 12) from the projectile, are considered in Fig. 7 at 300, 500, and 1000 (similar patterns were obtained at 750 and 1500 MeV/nucleon). A good achievement by the model and in particular the proper account of the dependence on bombarding energy, both for integral and isotopic distributions, is observed, both for the magnitude and position of the peak in the Z distribution. We note (not shown) that the modification proposed in this paper for the width parameter R in Eqs. (17)–(20) permits to notably improve on the description of the isotopic distribution for the lightest systems where the width as given by Eqs. (17)–(20) is about 25% smaller than the prescription of Ref. [27]. It would therefore be worth implementing the new width parameter R in

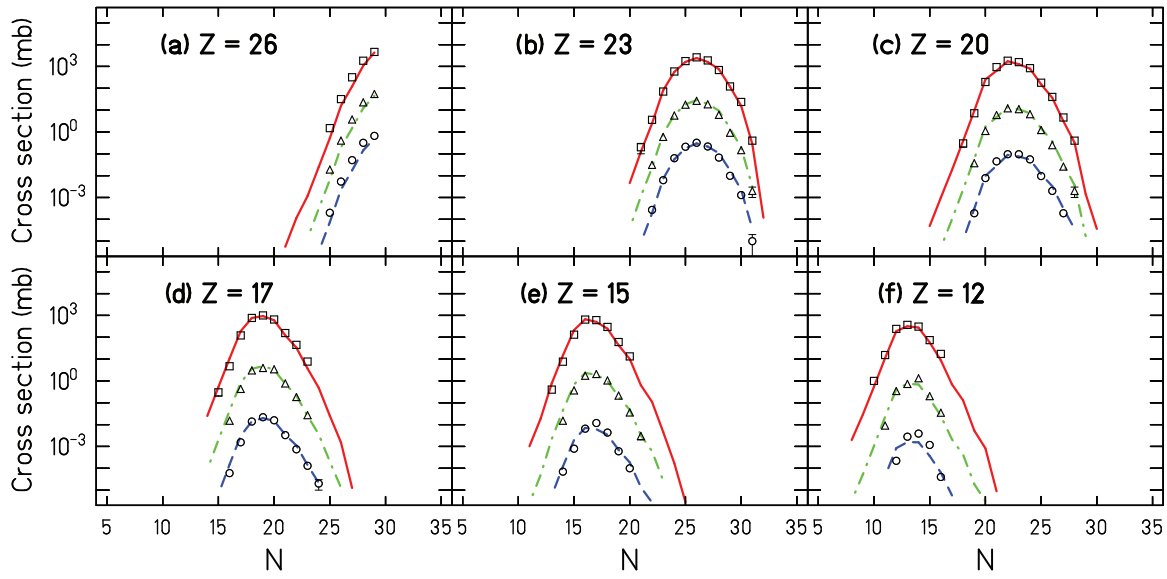

FIG. 7. (Color online) Sample of experimental isotopic distributions of the residues produced in the reactions induced by ^{56}Fe projectiles on a hydrogen target at 300-MeV/nucleon (circles), 500-MeV/nucleon (triangles), and 1000-MeV/nucleon (squares) beam energy [29,78]. Error bars are smaller than the symbols. For clarity, the data at 300 MeV/nucleon have been scaled by a factor of 10^{-2}, and those at 1000 MeV/nucleon have been scaled by a factor of 10^{2}. The measurements are compared to the predictions by SPACS (dashed blue, dashed-dotted green, and full red lines at 300, 500, and 1000 MeV/nucleon, respectively).

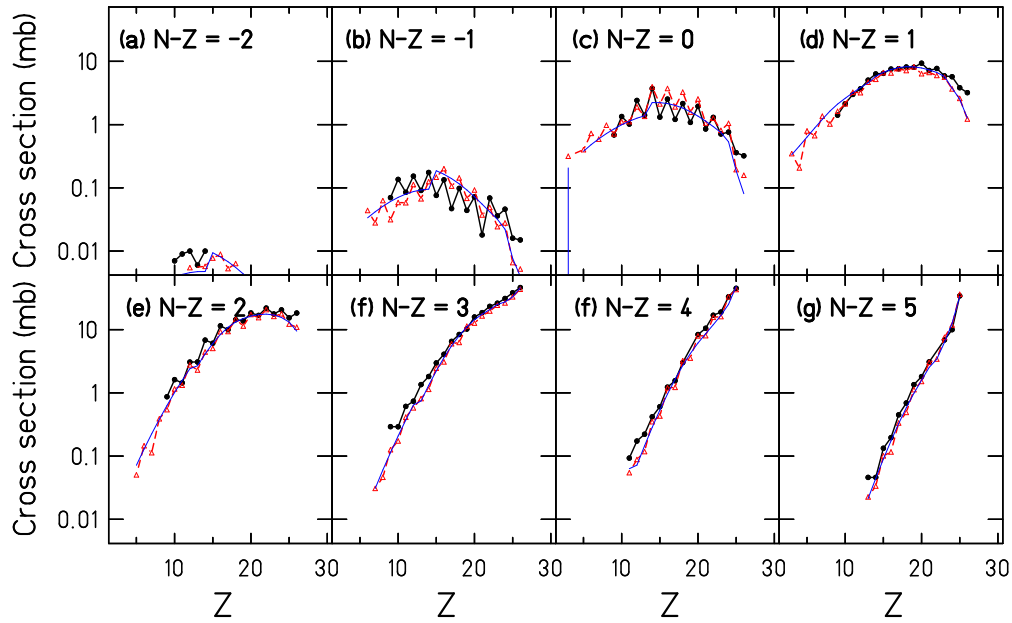

FIG. 8. (Color online) Experimental and calculated Z distributions of the residues produced in the reaction ^{56}Fe (1000 MeV/nucleon) + p for various selections in $(N - Z)$ from (a) $(N - Z) = -1$ to (g) $(N - Z) = +5$. The data are shown with black dots joined by full lines, whereas SPACS calculations are represented by red open circles joined by dashed lines. Model calculations without shell-structure and even-odd effects are also shown for comparison (thin blue lines). For clarity, experimental error bars are omitted.

other existing analytical parameterizations, independent on the entrance-channel reaction mechanism, and see whether it can help in improving the accuracy of the prediction there also.

The scale used in Figs. 6 and 7 provides a convenient overview of many systems and products simultaneously. Yet, structural effects and even-odd staggering if any are hardly visible. To best evidence such features, it was shown judicious to sort the data according to $(N - Z)$ [43]. For the reaction ^{56}Fe (1000 MeV/nucleon) + p, this idea is exploited in Fig. 8 where the production cross section is displayed as a function of the product atomic number Z for selections in $(N - Z)$ ranging from -2 to 5. The representation permits probing efficiently the achievement by the SPACS parameterization regarding the modeling of shell-structure and even-odd effects. It is observed that the prescription based on Eq. (27) is able to reproduce the magnitude of the staggering as well as its dependence on $(N - Z)$ rather well. The discrepancies which start to appear on the neutron-deficient wings of the lightest products are due to the contribution of other reaction mechanisms. The smooth thin blue lines in the figure correspond to calculations neglecting shell and even-odd effects [$F_{e\text{-}o}(A, Z) = 1$]. It serves as a reference and demonstrates the necessity of including staggering phenomena for a description in fine detail. Figure 8 shows that the analytical prescription developed in this paper is rather successful in this respect. According to the independence of the presently discussed shell-structure and pairing effects on the reaction mechanism [43,49,51–57], the modeling by means of Eqs. (27)–(33) may be useful for other analytical codes, too.

Fading out of shell-structure effects and pairing correlations due to the competition between particle evaporation and γ-ray emission and due to the influence of angular momentum is best illustrated with a heavy system. As a typical example, the isotopic distribution of $Z = 74$ products measured for the ^{208}Pb (1000 MeV/nucleon) + p already introduced above is considered in Fig. 9. Superimposed to the experimental data (black dots), three variants of the model calculations are shown: a calculation neglecting both γ-decay competition and angular momentum effects (blue squares), a calculation accounting for γ decay while neglecting angular momentum

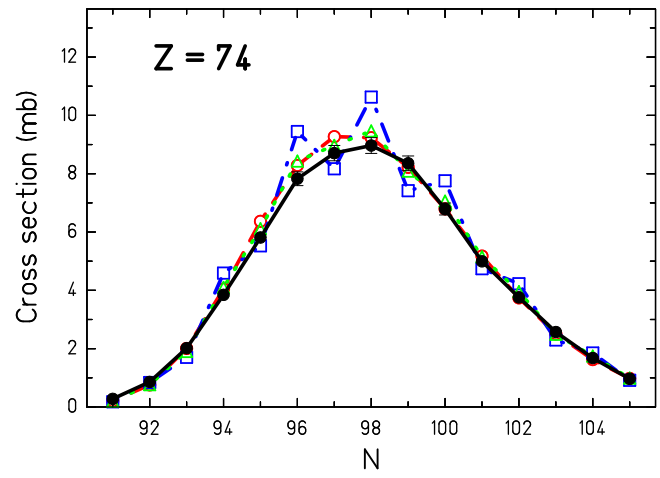

FIG. 9. (Color online) Isotopic distribution of element $Z = 74$ for the system ^{208}Pb (1000 MeV/nucleon) + p. The data are shown with black dots joined by a full line, together with three calculations: accounting for both γ-decay competition and angular momentum effects (red open circles joined by a dashed line), accounting for γ-decay competition but neglecting angular momentum effects (green open triangles joined by a dotted line), neglecting both γ-decay competition and angular momentum effects (blue open squares joined by a dashed-dotted line).

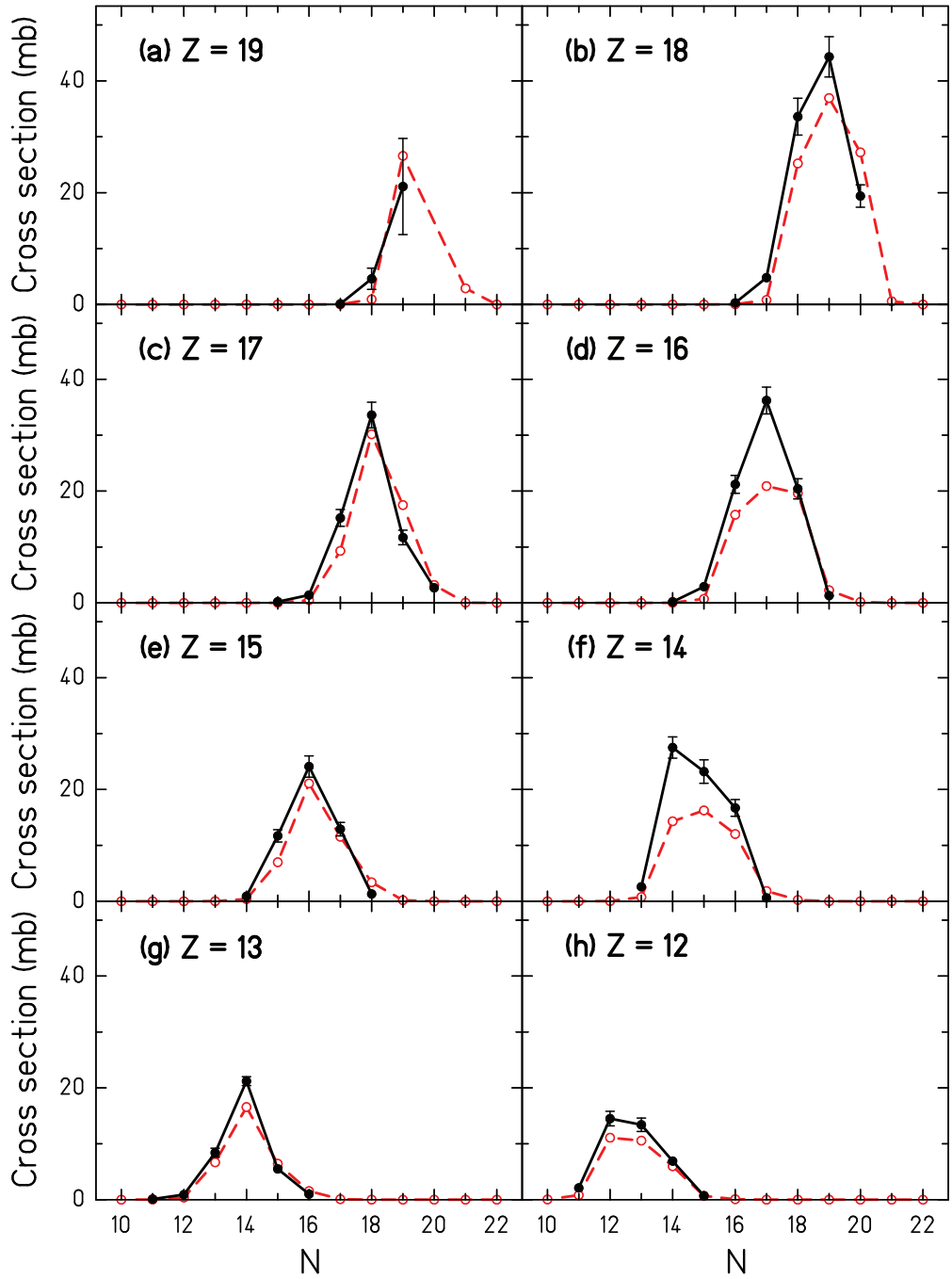

FIG. 10. (Color online) Sample of experimental isotopic distributions of the residues produced in the reactions induced by ^{40}Ca projectiles on a hydrogen target at 763 MeV/nucleon [80] (black dots joined by full lines). The measurement is compared to the predictions by SPACS (red open circles joined by dashed lines).

(green triangles), and a calculation accounting for both features (red circles). While the latter—most complete—calculation properly describes the structureless experimental distribution, the former two display a more or less strong staggering, inconsistent with the measurement. The figure illustrates how the reduction of staggering due to γ-ray emission and angular momentum, respectively, is implemented in SPACS.

Compiling the calculations performed along this section, one concludes to a good description by SPACS for spallation of iron to lead from 200 to 1500 MeV/nucleon bombarding energy. Among existing *analytical* parameterizations of the same kind, this is rather unique since SPACS involves a single set of equations, valid for any kind of reaction partner and product. On a more quantitative level, the precision of the calculation for the cross section of a given residue is, in general, below 15%. Larger discrepancies can nevertheless be reached in specific cases at the edges of the distribution. After having benchmarked the SPACS parameterization with the GSI data, we assess in the following sections its accuracy over a wider range in reaction-partner mass and bombarding energy.

B. Comparison with LBL data: from Ne to Ni from 350 to 900 MeV/nucleon

Spallation-residue (A, Z) production cross sections were measured in inverse kinematics at LBL Bevalac [31,79,80], where light and medium-mass systems (Ne, Ar, Ca, Cr, and Ni) were measured at various bombarding energies between 350 and 900 MeV/nucleon. A sample of these measurements is presented and compared with model predictions in Figs. 10 and 11.

Figure 10 focuses on the bombardment of hydrogen by a ^{40}Ca projectile at 763 MeV/nucleon. The isotopic distribution is displayed for a series of product elements. The experimental distribution is rather well reproduced by the calculation, including the manifestation of even-odd staggering. The production of a couple of elements is nonetheless clearly overestimated. For some isotopes, a discrepancy—amounting to a factor of 1.5 at most—is thus observed. A similar reasonable agreement was found for spallation involving ^{36,40}Ar projectiles, demonstrating the proper description of the dependence of the isotopic production on the N/Z of the projectile as implemented in SPACS.

Figure 11 considers the lightest projectile available in the LBL campaign with the reaction ^{22}Ne (894 MeV/nucleon) + p. This system permits assessing the precision of the analytical parameterization developed in this paper towards a domain of interest in astro- and biophysics. Although the experimental points are few, the achievement by the calculation is quite good. The slope of the Z distribution is quantitatively described, and the magnitude of structural and even-odd effects is reasonably well reproduced too. Also shown in Fig. 11 is a calculation without structural and even-odd staggering, demonstrating the crucial account of the latter for a description in finer detail. Remaining discrepancies are of the same magnitude as for the Ca, Ar + p reactions. We remind that such systems are out of the range of reactions used for adjusting the equations and parameters of the model.

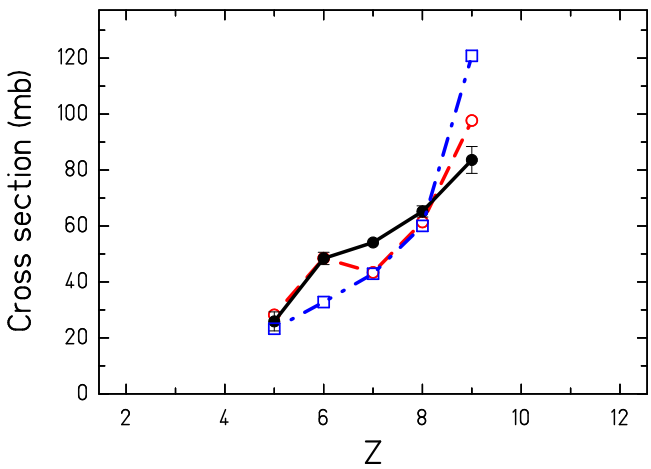

FIG. 11. (Color online) Experimental Z distribution of the residues produced in the reaction induced by ^{22}Ne projectiles on a hydrogen target at 894 MeV/nucleon [31]. The data (black dots joined by a full line) are compared to the predictions by SPACS with (red open circles joined by a dashed line) and without structural staggering (blue open squares joined by a dashed-dotted line).

The lack of complete data on the isotopic production for spallation of even lighter systems makes it difficult to firmly quantify the predictive power of SPACS in this region, and importantly, to establish the lower limit of applicability of the model in terms of reaction-partner mass. The above results are encouraging, and it would be interesting to test the parameterization towards lower masses and energies. Calculations on spallation of carbon, nitrogen, and oxygen, down to a few tens of MeV/nucleon bombarding energy, have been compared to the few available experimental points [81–83]. According to the scattered character of these points, we estimate the uncertainty of the prediction to lie within a factor of 2 to 3. Comparison of the calculation with recent measurements on spallation of ^{12}C at 95 MeV/nucleon [84,85] yields a slightly better achievement with a factor between calculation and experiment of around 1.5 on average.

C. Comparison with excitation functions measured in direct kinematics

To further probe the validity range and precision of SPACS, we compare the model predictions with experiments dedicated to excitation functions of individual residues. We consider in this paper the representative work by Kaufman *et al.* [86], Titarenko *et al.* [87–89], Leya *et al.* [90], and Belyaev *et al.* [91]. Measurements were performed in direct kinematics, and isotopic identification was achieved by off-line γ spectrometry in most cases. Contrary to the inverse-kinematics experiments considered in the previous sections, this technique is restricted to selected nuclides. Yet, it permitted so far to scan a larger variety of reaction-partner masses and bombarding energies. As a typical example, in Ref. [86] the excitation function of specific products was established in spallation of ^{197}Au from 200 to 6000 MeV/nucleon, and in Refs. [87–89] excitation functions were extended down to 40 MeV/nucleon for spallation of Fe, Ni, Nb, W, Ta, Pb, and Bi. The direct- and inverse-kinematics methods thus constitute fully complementary approaches.

A set of excitation functions from the above-quoted references is compared to SPACS predictions in Fig. 12. We restrict to product nuclides for which independent yields are available, allowing most direct comparison to the model calculation.[5] Although we observed that some discrepancy can appear below a few tens of MeV/nucleon, the description of the shape of the experimental excitation function by the analytical model is rather good for Bi down to Si from energies down to 50 MeV/nucleon. A more quantitative investigation shows that, depending on the reaction and nuclide product, the agreement goes from within a few percents to a factor of up to 2 to 5 [see panels (c), (d), (f), and (i)]. The discrepancy appears sometimes at the edge of the isotopic (isobaric) distribution, which may be the consequence of a shift by 0.5 to 1 unit in mass (charge) of the calculated distribution as compared to the experimental one. Nevertheless, this is not systematic, and as

[5]Cumulative yields are affected by the production rate of precursor nuclei in the radioactive decay chain. Comparison with calculations thus requires an involved unfolding procedure, which is out of scope of this paper.

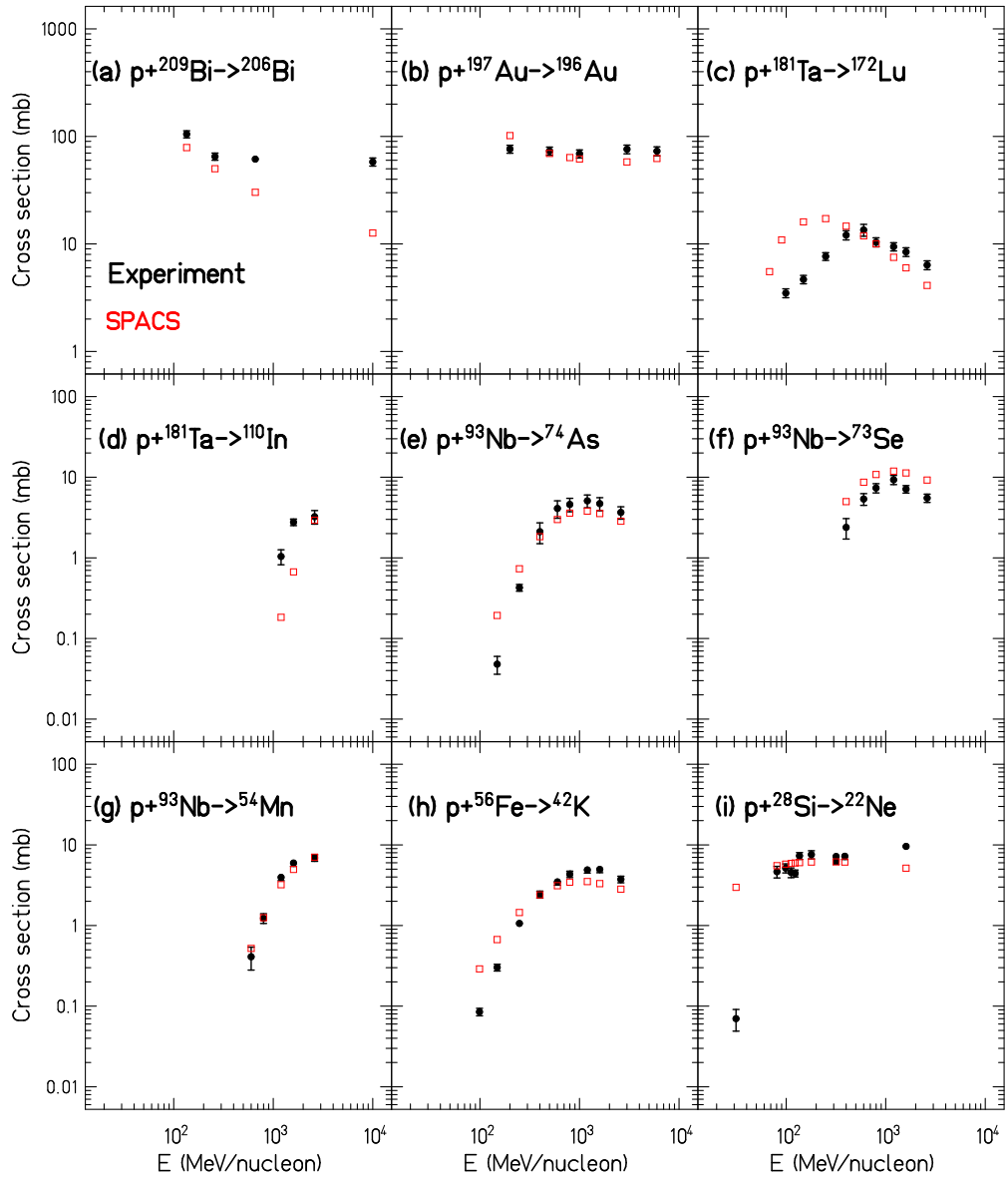

FIG. 12. (Color online) Excitation function of ^{206}Bi, ^{196}Au, ^{188}Pt, ^{183}Re, ^{181}Re, ^{175}Hf, ^{167}Tm, and ^{149}Tm produced in direct-kinematics experiments with the indicated reactions. The experimental data [87–91] are shown by black dots; error bars are smaller than the symbols wherever not visible. The predictions by SPACS are displayed by open red squares.

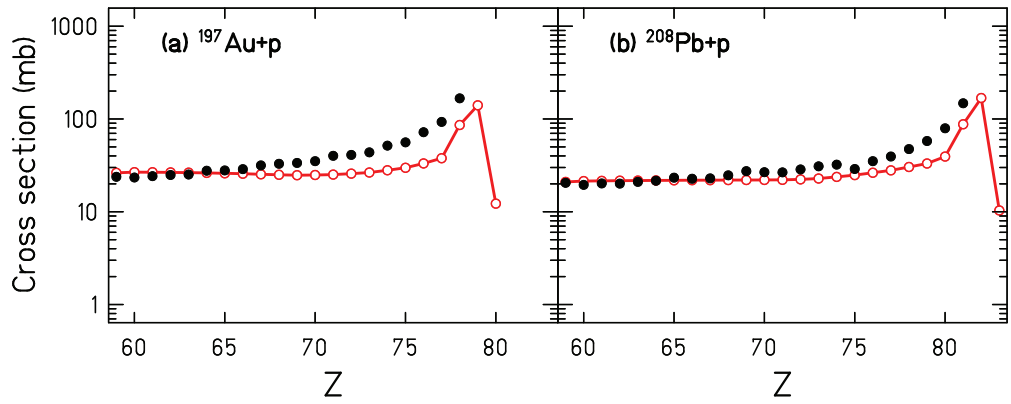

FIG. 13. (Color online) Element distributions of the residues produced in reactions induced by ^{197}Au at 10.6 GeV/nucleon (left panel) and ^{208}Pb at 158 GeV/nucleon on hydrogen. Experimental cross sections [23,92] (black dots) are compared to predictions by SPACS (red circles joined by lines). Error bars are not shown for clarity; they are smaller than the symbols in most cases.

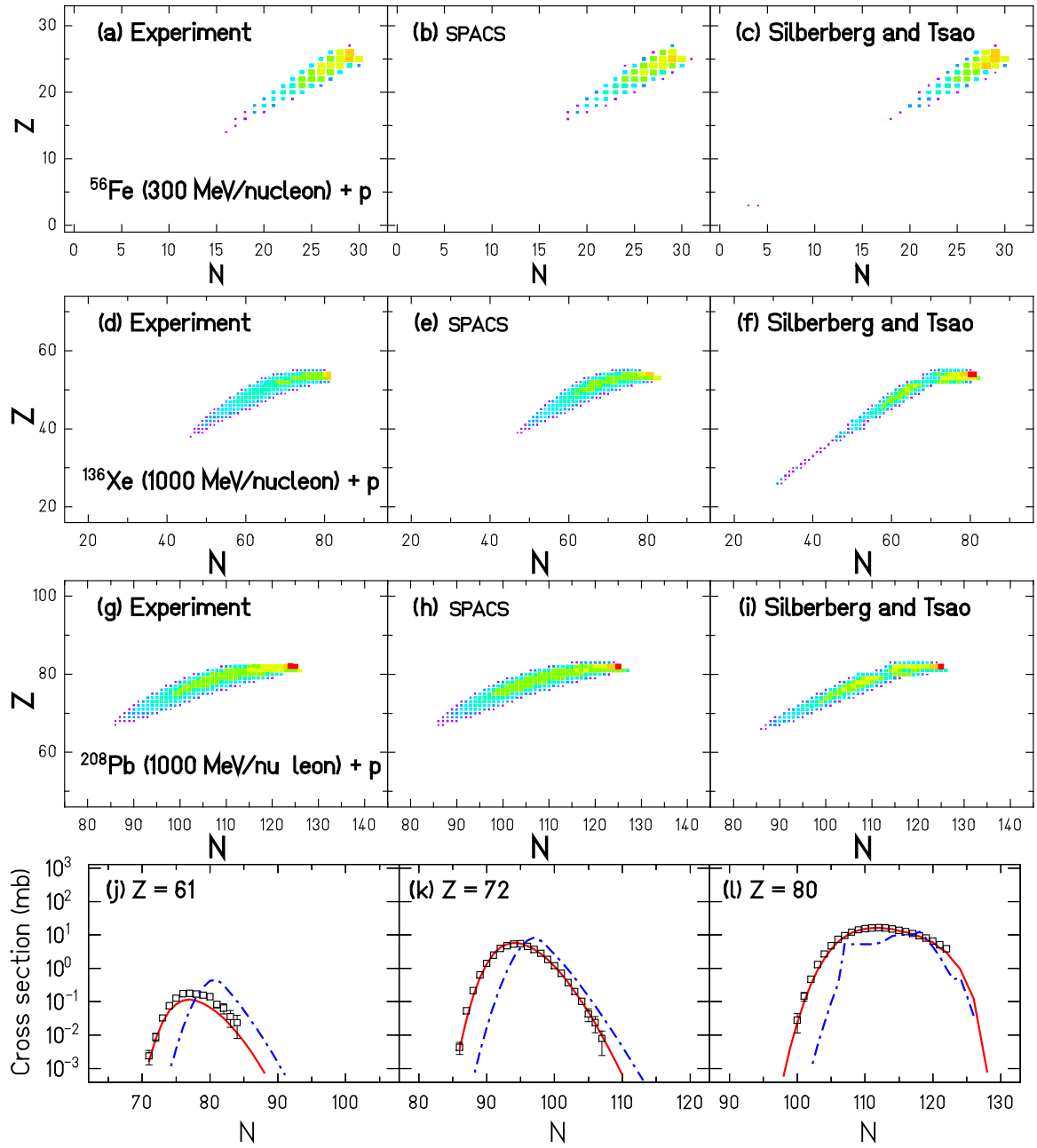

FIG. 14. (Color online) First row: Chart of the nuclides produced in the interaction of ^{56}Fe on hydrogen at 300 MeV/nucleon: Experimental data from Ref. [29] (left), predictions by SPACS (middle) and predictions by the parameterization of Silberberg and Tsao [14] and Barghouty [93] (right). Second row: Identical to the first row for ^{136}Xe on hydrogen at 1000 MeV/nucleon. The data are from Ref. [77]. Third row: Identical to the first row for ^{208}Pb on hydrogen at 1000 MeV/nucleon. The data are from Ref. [70]. Fourth row: Isotopic distributions of element $Z = 61$ (left), $Z = 72$ (middle), and $Z = 80$ (right) produced in ^{208}Pb (1000 MeV/nucleon) + p. The data (open squares) are compared to predictions by SPACS (full red line) and predictions by Silberberg and Tsao (dashed-dotted blue line).

will be seen in Sec. III E below, the wings of the distributions can be remarkably well described in many cases. Hence, part of the discrepancy observed in Fig. 12 remains unexplained, and further investigations are required to enlighten the point.

D. Behavior at very high up to ultra-relativistic energies

For astrophysical issues involving ultraheavy cosmic-ray nuclei ($Z > 30$), the energy domain of interest largely exceeds 1000 MeV/nucleon. In the likely absence of a limiting-fragmentation-like regime for spallation in the energy range of current facilities, it is of importance to provide predictions that properly account for the energy dependence up to high values. Calculations of cosmic-ray propagation in the interstellar medium will be very sensitive to this aspect [6]. Figure 13 compares the predictions of SPACS with data collected for the systems ^{197}Au + p [23] (left) and ^{208}Pb + p [92] (right) at 10.6 and 158 GeV/nucleon, respectively. The agreement between

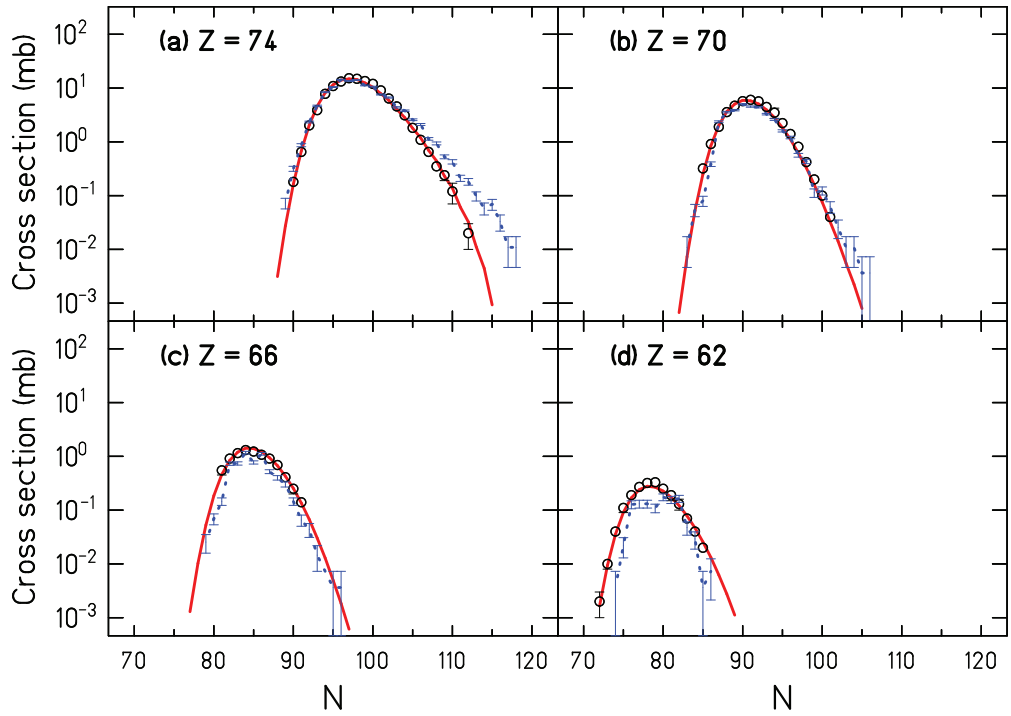

FIG. 15. (Color online) Sample of experimental isotopic distributions of the residues produced in the reactions induced by ^{197}Au projectiles on a hydrogen target at 800-MeV/nucleon beam energy [48] (circles). The measurement is compared to the predictions by INCL4.6-ABLA07 (dotted blue lines) [97] and to those by SPACS (full red lines). Wherever not visible, the experimental error bars are smaller than the symbols. The error bars of the Monte Carlo simulation are of statistical nature.

calculation and experiment is observed to be satisfactory: The discrepancy amounts to a factor of 3, at most, for the integral Z (equivalently, A) distribution. This result, together with the comparisons performed in the previous sections, gives further confidence into the reasonable form of the energy dependence as implemented in SPACS.

E. Comparison with other models

In this section, we compare the new parameterization to an existing analytical prescription as well as to a Monte Carlo calculation.

The utility of SPACS is first illustrated in Fig. 14. In the three upper rows, the production of heavy residues by spallation of a light [panels (a)–(c)], a medium [panels (d)–(f)], and a heavy [panels (g)–(i)] system is represented on the top of the (N, Z) chart of nuclides. A more quantitative comparison is made in the last row [panels (j)–(l)] where projections on the N axis for selected elements are shown for the heavy system. The experimental data are compared with the predictions by an updated version of the Silberberg and Tsao prescription [93] and the predictions by SPACS. The parameterization of Silberberg and Tsao is the most widespread analytical model in the field, and it is used for many applications [94]. However, due to limited accuracy, some authors (see, e.g., Refs. [95,96]) preferred to abandon analytical solutions and go for Monte Carlo models at the price of larger computing time. Figure 14 shows that, although both calculations describe the data reasonably well for ^{56}Fe (300 MeV/nucleon) + p, SPACS is observed to perform better as the size of the system gets larger. As mentioned in the Introduction, the deficiency of previous parameterizations may for a large part be attributed to the limited amount and accuracy of the data available at the time they were developed. Their reliability outside of the range of the fit is thus even the more hazardous. According to the set of comparisons made in this paper, the SPACS parameterization is expected to provide more realistic results for heavy systems and as reliable predictions for light ones as compared to the Silberberg and Tsao formalism.

The interest in the availability of the semi-empirical parameterization developed in this paper is additionally assessed by comparing its achievement with an elaborate Monte Carlo model of the kind available today in the field [62,30]. In Fig. 15 a sample of experimental spallation-residue isotopic distributions from ^{197}Au (800 MeV/nucleon) + p [48] (see also Fig. 4) is superimposed to the predictions by the latest version of the INCL4.6-ABLA07 code [97] and those by SPACS. The analytical prescription follows quite well the INCL4.6-ABLA07 distributions. For several elements, SPACS even better describes the experiment down to the edge of the distributions. Thus, the analytical model developed in this paper can be used as a fast mean for predicting cross sections of weakly populated exotic isotopes for which Monte Carlo physical methods require high statistics.

IV. SUMMARY AND CONCLUSIONS

A new semi-empirical parameterization named SPACS for the calculation of residue-production cross sections in proton- and neutron- induced spallation reactions from the Fermi

regime to ultra-relativistic energies for light up to heavy systems is presented. The basic ideas are similar to those of existing parameterizations, whereas a new prescription is developed for modeling the mass yield and which explicitly accounts for the dependence of the product yield on the bombarding energy. The description of the isobaric distribution profits from the formalism used in the well-known parameterization for fragmentation EPAX. Suitable modifications were nonetheless introduced for matching the specificities of the spallation mechanism on one side and improving upon some aspects of EPAX on the other side. A dedicated analytical modeling of shell-structure and pairing correlation effects, based on the lowest particle energy threshold at the late stage of the deexcitation process, is developed and implemented in such a code for the first time. The influence of γ-ray emission along the cascade as well as of the angular momentum of the product fragment, which both attenuate structural staggering, are also parameterized. Finally, the nucleon-nucleus total reaction cross section, required to normalize the product yields, is borrowed from a recently developed prescription after suited modifications.

The comprehensive data set collected over the past decades at GSI, Darmstadt, including a wide domain in system size and bombarding energy, is used to adjust the model parameters. The parameterization is further benchmarked with independent experimental results involving a larger palette of systems and energies, measured at various facilities, and with diverse techniques. Along this comparison, the semi-empirical parameterization SPACS is shown to properly describe the dependence of the production cross sections on the system size, neutron-proton asymmetry N/Z, and energy. The modeling of shell-structure- and pairing-driven staggerings, as analytically implemented in SPACS, permits describing the experimental data in further richness and detail. The prescription of the structural effects developed in this paper is independent of the entrance channel and can thus be implemented in existing parameterizations of mechanisms as various as binary-decay processes, intermediate-fragment emission, heavy-ion fragmentation, and multi-fragmentation-like phenomena.

The development of the semi-empirical parameterization for spallation cross sections makes available a global prescription for neutron- and proton-induced spallation with a limited number of parameters valid for ions with $A \sim (12 - 200)$ and energies above $\sim$50 MeV/nucleon. Most successful existing empirical parameterizations and parametric fits involve a huge amount of formulas and parameters with uncertain predictive power outside the range of their adjustment. The comparison to experiment conducted in this paper supports the quite robust achievement by SPACS over a wide domain with a universal set of parameters. The accuracy of the predictions is below 20% (in most cases, much better) for spallation of ions above iron and energies above about 300 MeV/nucleon. The uncertainty can reach a factor of (1.5–5) for lighter systems or ultra-relativistic energies, not too far down in the wings of the distributions. Its features make SPACS a relevant fast and reliable tool for use in simulations in nuclear-, astro-, and biophysics.

ACKNOWLEDGMENTS

We would like to thank A. Boudard and D. Mancusi for providing the INCL4.6-ABLA07 calculations and related discussion. M.-V. Ricciardi, K. Sümmerer, and D. Cussol are acknowledged for fruitful discussions. We are grateful to L. Tassan-Got and C. Paradela for allowing us to use the ^{136}Xe + p data at 200 MeV/nucleon prior to publication. This work was supported by the French-German collaboration between IN2P3-DSM/CEA and GSI, under Agreement No. 04–48.

APPENDIX

For the practitioner user, a self-sufficient summary of the SPACS formalism, equations, and numerical values of the parameters is proposed in this Appendix. Also, an executable version as well as the software are made free available on request by the authors. We remind that SPACS is intended to describe spallation-residue isotopic production cross sections. It applies to proton- and neutron-induced spallation on light (around C) up to heavy (Pb, Bi) nuclei, over an energy range from around 50 MeV/nucleon to a few hundred GeV/nucleon. Hereafter, we adopt the convention of inverse kinematics. Application to direct kinematics straightforwardly requires interchanging the terms $A_{\rm proj}$ and $A_{\rm tar}$ in the formulas. Considering such a convention, ($A_{\rm tar} = 1$, $Z_{\rm tar} = 0$) and ($A_{\rm tar} = 1$, $Z_{\rm tar} = 1$) for neutron- and proton-induced reactions, respectively.

The production cross section of a nuclide of mass A and charge Z for nucleon-induced spallation of a nucleus of mass $A_{\rm proj}$, nuclear charge $Z_{\rm proj}$, and at incident energy $E_{\rm proj}$ (in MeV/nucleon), is computed as follows:

$$\sigma(A,Z) = \sigma_R Y(A) Y(Z_{\rm prob} - Z)|_A. \tag{A1}$$

1. Mass yield

$$Y(A) = Y(A)_{\rm cent} + Y(A)_{\rm periph}, \tag{A2}$$

with

$$Y(A)_{\rm cent} = [A_{\rm length}/(1 + \exp\{[(A_{\rm proj} - A_{\rm cent}) - A]\})]/A_{\rm cent}, \tag{A3a}$$

$$Y(A)_{\rm periph} = A_{\rm periph} \exp\{[A - (A_{\rm proj} - A_{\rm diff})]/A_{\rm diff}\}(E_{\rm proj}/1000)^{B_{\rm periph}}/A_{\rm cent}. \tag{A3b}$$

a. Central collision contribution

$$A_{\rm cent} = \alpha_{\rm cent}/\exp(A_{\rm proj}/\beta_{\rm cent}), \tag{A4}$$

supplemented with

$$A_{\rm cent} = A_{\rm proj}\{1 - \exp[-\ln(A_{\rm cent})/\ln(A_{\rm proj})(E_{\rm proj}/1000)^{\varepsilon_{\rm cent}}]\}. \quad \text{(A5)}$$

$$\text{for} \quad A > (A_{\rm proj} - A_{\rm cent} + \alpha_{\rm length} A_{\rm cent\_fluct})$$

$$A_{\rm length} = \sqrt{[(A_{\rm cent} + \alpha_{\rm length} A_{\rm cent\_fluct})^2 - (A_{\rm proj} + \alpha_{\rm length} A_{\rm cent\_fluct} - A_{\rm cent} - A)^2]}/(A_{\rm cent} + \alpha_{\rm length} A_{\rm cent\_fluct}),$$

$$\text{for} \quad A \leqslant (A_{\rm proj} - A_{\rm cent} + \alpha_{\rm length} A_{\rm cent\_fluct}), \quad A_{\rm length} = 1. \quad \text{(A6)}$$

$$A_{\rm cent\_fluct} = a_{\rm fluct} A_{\rm cent}^{\delta_{\rm fluct}} (E_{\rm proj}/1000)^{\varepsilon_{\rm fluct}}, \quad \text{(A7)}$$

with

$$a_{\rm fluct} = \alpha_{\rm fluct} + \beta_{\rm fluct} A_{\rm proj}. \quad \text{(A8)}$$

Numerical overflow exception for $(A_{\rm cent} + \alpha_{\rm length} A_{\rm cent\_fluct}) > 19$: $(A_{\rm cent} + \alpha_{\rm length} A_{\rm cent\_fluct}) = 19$ in Eq. (A6).

b. Peripheral collision contribution

$$A_{\rm periph} = \alpha_{\rm periph} + \beta_{\rm periph} A_{\rm proj}, \quad \text{(A9)}$$

with

$$A_{\rm diff} = \alpha_{\rm diff} + \beta_{\rm diff} A_{\rm proj}, \quad \text{(A10)}$$

$$B_{\rm periph} = \gamma_{\rm periph}[1 + \exp(-\{[\ln(1000)/\ln(E_{\rm proj})]^6 + \varepsilon_{\rm periph}\}/\delta_{\rm periph})]. \quad \text{(A11)}$$

Numerical underflow exception for $[A - (A_{\rm proj} - A_{\rm diff})]/A_{\rm diff} < -50$: $[A - (A_{\rm proj} - A_{\rm diff})]/A_{\rm diff} = -50$ in Eq. (A3b).

2. Charge dispersion

$$Y(Z_{\rm prob} - Z)|_A = n \ \exp(-R|Z_{\rm prob} - Z|^{U_n})$$

$$\text{for} \quad (Z_{\rm prob} - Z) > 0. \quad \text{(A12a)}$$

$$Y(Z_{\rm prob} - Z)|_A = n \ \exp(-R|Z_{\rm prob} - Z|^{U_p})$$

$$\text{for} \quad (Z_{\rm prob} - Z) \leqslant 0, \quad \text{(A12b)}$$

with

$$n = \sqrt{(R/\pi)}, \quad \text{(A13)}$$

$$Z_{\rm prob} = Z_\beta + \Delta + \Delta_m^{n,p} + 0.002A, \quad \text{(A14)}$$

$$Z_\beta = A/(1.98 + 0.0155A^{2/3}), \quad \text{(A15)}$$

$$Z_{\beta p} = A/\left(1.98 + 0.0155A_{\rm proj}^{2/3}\right). \quad \text{(A16)}$$

Numerical underflow exception for $(-R|Z_{\rm prob} - Z|^{U^p}) > -70$: $(-R|Z_{\rm prob} - Z|^{U^p}) = -70$ in Eq. (A12b).

a. Most probable nuclear charge

$$\text{for} \quad A \geqslant \Delta_6, \quad \Delta = \Delta_1 + \Delta_2 A + \Delta_3 A^2 + \Delta_4 A^3,$$

$$\text{for} \quad A < \Delta_6, \quad \Delta = \Delta_5 A^2. \quad \text{(A17)}$$

$$\text{for} \quad A/A_{\rm proj} > d_2 \quad \text{and} \quad A/A_{\rm proj} \leqslant d_3, \quad \Delta = \Delta[1 + d_1(A/A_{\rm proj} - d_2)^2],$$

$$\text{for} \quad A/A_{\rm proj} > d_2, \quad \Delta = \Delta[1 + d_1(A/A_{\rm proj} - d_2)^2 + d_4(A/A_{\rm proj} - d_3)^3]. \quad \text{(A18)}$$

$$\text{for} \quad (Z_{\rm proj} - Z_{bp}) \leqslant 0 \text{ (neutron-rich projectile)},$$

$$\Delta_m^n = \{n_1(A/A_{\rm proj})^6 + n_2[(A_{\rm proj} - A)/A_{\rm proj}]^2\} \times (Z_{\rm proj} - Z_{\beta p}), \quad \text{(A19)}$$

$$\text{for} \quad (Z_{\rm proj} - Z_{bp}) > 0 \text{ (proton-rich projectile)},$$

$$\Delta_m^p = [\exp(p_1 + p_2 A/A_{\rm proj})](Z_{\rm proj} - Z_{\beta p}),$$

supplemented with

$$\Delta_m^p = \Delta_m + p_3[(A_{\rm proj} - A)/A_{\rm proj}]^2(Z_{\rm proj} - Z_{\beta p})$$

$$\text{for} \quad A/A_{\rm proj} < 0.5, \quad \text{(A20a)}$$

$$\Delta_m^p = \Delta_m + \{\exp[-(d_3 - A/A_{\rm proj})^2/0.005]\} \times (Z_{\rm proj} - Z_{\beta p}) \quad \text{for} \quad A \geqslant \Delta_6. \quad \text{(A20b)}$$

b. Charge-distribution width

For $A < t_1$,

$$R^{\rm phy} = R_0^{n,p} \ \exp\{-\ln[R_1(A/t_2)]\}, \quad \text{(A21)}$$

for $A \geqslant t_1$,

$$R^{\rm phy} = R_0^{n,p} \exp(R_2 + R_3 A + R_4 A^2).$$

For $(Z_{\rm proj} - Z_{\beta p}) \leqslant 0$ (neutron-rich projectile),

$$R_0^n = r_0 \ \exp[r_3(Z_{\rm proj} - Z_{\beta p})], \quad \text{(A22)}$$

for $(Z_{\rm proj} - Z_{\beta p}) > 0$ (proton-rich projectile),

$$R_0^p = r_0 \ \exp[r_4(Z_{\rm proj} - Z_{\beta p})], \quad \text{(A23)}$$

$$\text{for} \quad i = 2 - 4 : R_i = r_{i,0} + r_{i,1}|Z_{\rm proj} - Z_{\beta p}|, \quad \text{(A24)}$$

$$\text{for} \quad A < t_1 \text{ and } A/A_{\rm proj} < r_2 : \quad R = 1/[2(1/(2R^{\rm phy}) + \sigma_{\rm fluct}^2)], \quad \text{(A25)}$$

$R = R^{\rm phy}$ otherwise

$$\text{for} \quad A/A_{\rm proj} \geqslant r_2, \quad R' = R \exp[r_1 - \sqrt{A_{\rm proj}(A/A_{\rm proj} - r_2)^5}]. \quad \text{(A26)}$$

Numerical limit for $\exp[r_1\sqrt{A_{\rm proj}(A/A_{\rm proj} - r_2)^5}] > 1$: $R' = R$ in Eq. (A26).

c. Charge-distribution fall off

$$U^n = u_{n1} + u_{n2}\, A/A_{\rm proj}, \tag{A27}$$

$$U^p = u_{p1} + u_{p2} A_{\rm proj}. \tag{A28}$$

d. Additional correction factors

$$Y(Z_{\rm prob} - Z)|_A = Y(Z_{\rm prob} - Z)|_A\, f_{n,p}, \tag{A29}$$

for $(Z_\beta - Z) > (Z_{\rm proj} - Z_{\beta p} + b_2)$,

$$f_n = 10^{[-b1\,|Z_{\rm proj} - Z\beta p|(Z_{\beta-Z} + Z_{proj} - Z_{\beta p} + b_2)^3]}, \tag{A30}$$

$$f_n = 1 \text{ otherwise}$$

for $Z > Z_{\rm exp}$, $f_p = 1/[10(dF/dZ)^{(Z - Z_{\rm exp})}]$, (A31)

with

$$dF/dZ = 1.2 + 0.647(A/2)^{0.3} \text{ and}$$

$$Z_{\rm exp} = Z_{\rm prob} + dF/dZ \ \ln(10)/(2R). \tag{A32}$$

e. Charge-exchange channel

$$Y(Z_{\rm prob} - Z)|_A = Y(Z_{\rm prob} - Z)|_A\, f_{pu}, \tag{A33}$$

for $E_{\rm proj} < 1000$ MeV/nucleon,

$$f_{pu} = a_{pu} + b_{pu} \exp[-(E_{\rm proj}/1000)/c_{pu}], \tag{A34}$$

$$f_{pu} = 1 \text{ otherwise.}$$

3. Modulation by structural effects and even-odd staggering

$$\sigma(A,Z) = \sigma(A,Z) F_{e\text{-}o}(A,Z), \tag{A35}$$

$$F_{e\text{-}o}(A,Z) = S_{\rm lpet}(A,Z)^{\rm EMP}/S_{\rm lpet}(A,Z)^{\rm MAC}, \tag{A36}$$

with $S_{\rm lpet}(A,Z)^{\rm EXP}$ and $S_{\rm lpet}(A,Z)^{\rm CALC}$ as the empirical and macroscopic lowest particle energy thresholds, respectively, of the product (A, Z).

The empirical lowest particle energy threshold is determined from experimental separation energies of Ref. [63]. The macroscopic lowest particle energy thresholds $S_{\rm lpet}(A, Z)^{\rm MAC}$ are obtained from the Thomas-Fermi masses [64] without shell-effect and pairing correlations. For unavailable experimental masses, Thomas-Fermi predictions [64] are used for $S_{\rm lpet}(A, Z)^{\rm EMP}$. In the rare cases where experiment and theory yield a different type of particle having the lowest binding energy, the experimental result defines the less bound particle to be used in Eq. (A35). Neutrons, protons, and α particles are considered only, and we restrict to ground-state-to-ground-state decays. Empirical and macroscopic separation energies are beforehand corrected by the Coulomb barrier B,

$$\text{for} \quad \text{protons}: B_p = 1.44(Z-1)/\{1.87[(A-1)^{1/3} + 1]\}, \tag{A37a}$$

$$\text{for} \quad \alpha \text{ particles}: B_\alpha = 1.44(Z-2)/\{1.87[(A-4)^{1/3} + 4^{1/3}]\}. \tag{A37b}$$

Numerical limit, if $F_{e\text{-}o}(A,Z) > 2 : F_{e\text{-}o}(A,Z) = 2$ in Eq. (A35).

a. Attenuation by γ-ray emission

$$F^\gamma_{e\text{-}o}(A,Z) = \exp\{\ln[F_{e\text{-}o}(A,Z)](1 - C_\gamma P_\gamma)\}, \tag{A38}$$

$$P_\gamma = \Gamma_\gamma/(\Gamma_n + \Gamma_p + \Gamma_\alpha + \Gamma_\gamma), \tag{A39}$$

with

$$\Gamma_\gamma = 0.62410^{-9} A^{1.6} T^5, \tag{A40a}$$

$$\Gamma_n = C_n (A-1)^{2/3} T/[1/T \exp(S_n/T)], \tag{A40b}$$

$$\Gamma_{p,\alpha} = C_{p,\alpha}(A - 1{,}4)^{2/3}[2T^2/(2T + B_{p,\alpha})] /\{1/T \exp[(S_{p,\alpha} + B_{p,\alpha})/T]\}, \tag{A40c}$$

$$T = A^{-2/3}/(0.057 + 0.00193\delta U), \tag{A41}$$

$$C_p = 938.3/939.6 C_n, \tag{A42a}$$

$$C_\alpha = 3727.4/939.6 C_n, \tag{A42b}$$

where $S_{n,p,\alpha}$ are the separation energies from Ref. [63] and δU are the shell corrections from Ref. [64].

Numerical limits:
if $T \leqslant 0$ or $S_n \geqslant 50$ or $A \leqslant 1 : \Gamma_n = 0$ in Eq. (A40b),
if $T \leqslant 0$ or $S_p \geqslant 50$ or $A \leqslant 1 : \Gamma_p = 0$ in Eq. (A40c),
if $T \leqslant 0$ or $S_n \geqslant 50$ or $A \leqslant 4 : \Gamma_\alpha = 0$ in Eq. (A40c).

b. Attenuation caused by angular-momentum effects

$$F^{\gamma,L}_{e\text{-}o}(A,Z) = F^\gamma_{e\text{-}o}(A,Z)/[1 + (J - J_{cr})/D_J], \tag{A43}$$

$$J = (\sqrt{\sigma^2} - 0.5), \tag{A44}$$

TABLE I. Constants used in SPACS for the parameterization of the mass yield.

Parameter	Constant	Value
Mass loss in central collisions	$\alpha_{\rm cent}$	1.39
	$\beta_{\rm cent}$	1560
	$\varepsilon_{\rm cent}$	0.75
	$\alpha_{\rm length}$	0.7
Fluctuations in mass loss	$\alpha_{\rm fluct}$	7.876
	$\alpha_{\rm fluct}$	−0.0066
	$\delta_{\rm fluct}$	0
	$\varepsilon_{\rm fluct}$	0.5
Peripheral collisions	$\gamma_{\rm periph}$	0.9
	$\alpha_{\rm periph}$	0.905
	$\beta_{\rm periph}$	-9.868×10^{-4}
	$\varepsilon_{\rm periph}$	−0.05
	$\delta_{\rm periph}$	0.065
	$\alpha_{\rm diff}$	1.572
	$\beta_{\rm diff}$	−0.00132

with

$$\sigma^2 = 0.16A^{2/3}(A_{\rm proj} - A)(2A_{\rm proj} + A)/[9(A_{\rm proj} + 1)]. \quad \text{(A45)}$$

Applicability range

$$\text{for} \quad A = A_{\rm proj} \text{ and } Z = Z_{\rm proj} : \sigma(A,Z) = 0,$$
$$\text{for} \quad Z > Z_{\rm proj} + 2 : \sigma(A,Z) = 0,$$
$$\text{for} \quad A > A_{\rm proj} : \sigma(A,Z) = 0.$$

TABLE II. Constants used in SPACS for the description of the charge-dispersion curve.

Parameter	Constant	Value
$Z_{\rm prob}$ shift	Δ_1	-1.3327
	Δ_2	0.05368
	Δ_3	-2.058×10^{-4}
	Δ_4	4.9639×10^{-7}
	Δ_5	1.9×10^{-4}
	Δ_6	131
	d_1	-25
	d_2	0.8
	d_3	0.9
	d_4	-95
n-rich memory effect	n_1	1.2
	n_2	0.4
p-rich memory effect	p_1	-11.25
	p_2	11.0
	p_3	-0.75
Width R	t_1	98
	t_2	112
	R_1	3.65
	r_0	2.78
	r_1	2800
	r_2	0.86
	r_3	0.0212
	r_4	0.178
	$r_{2,0}$	1.8122
	$r_{2,1}$	-4.4807
	$r_{3,0}$	0.01638
	$r_{3,1}$	-0.07932
	$r_{4,0}$	-1.0624×10^{-4}
	$r_{4,1}$	3.41181×10^{-4}
	$\sigma_{\rm fluct}$	0.35
n-rich slope U^n	u_{n1}	0.934
	u_{n2}	0.9984
p-rich slope U^p	u_{p1}	2.1
	u_{p2}	0.0013
n-richness correction	b_1	0.0023
	b_2	2.4
Charge exchange	a_{pu}	0.34508
	b_{pu}	4.27305
	c_{pu}	0.53384

4. Normalization

$$\sigma_R \text{ (mbarns)} = \pi 10 r_0^2 \left(A_{\rm proj}^{1/3} + A_{\rm tar}^{1/3} + \delta_{\rm E}\right)^2 \times (1 - B/E_{CM})\chi_m \quad \text{for} \quad E_{CM} \geqslant B \quad \text{(A46)}$$

with $r_0 = 1.1$ fm.

Sub-barrier interactions being not treated, $\sigma_R = 0$ for $E_{CM} < B$,

$$B = 144 Z_{\rm tar} Z_{\rm proj}/R, \quad \text{(A47)}$$

$$E_{CM} = E_{\rm proj} A_{\rm proj}/(A_{\rm proj} + A_{\rm tar}) \quad \text{with} \quad E_{\rm proj} \text{ in MeV/nucleon}, \quad \text{(A48)}$$

$$R = r_{\rm tar} + r_{\rm proj} + 1.2\left(A_{\rm proj}^{1/3} + A_{\rm tar}^{1/3}\right)/E_{cm}^{1/3}. \quad \text{(A49)}$$

with

$$r_{\rm tar} = 1.29 r_{\rm tar}^{\rm rms} \quad \text{(A50a)}$$

where

$$r_{\rm tar}^{\rm rms} = 0.85 \text{ for } Z > 0 \text{ and } r_{\rm tar}^{\rm rms} = 0.34 \text{ for } Z < 1,$$
$$r_{\rm proj} = 1.29 r_{\rm proj}^{\rm rms} \quad \text{(A50b)}$$

where

$$r_{\rm proj}^{\rm rms} = 0.891 A_{\rm proj}^{1/3}(1 + 1.565 A_{\rm proj}^{-2/3} - 1.04 A_{\rm proj}^{-4/3}),$$
$$\delta_E = 1.85 S + \left(0.16 S/E_{CM}^{1/3}\right) - C_E + 0.91(A_{\rm proj} - 2Z_{\rm proj})Z_{\rm tar}/(A_{\rm proj}A_{\rm tar}), \quad \text{(A51)}$$
$$S = A_{\rm tar}^{1/3.} A_{\rm proj}^{1/3}/\left(A_{\rm tar}^{1/3} + A_{\rm proj}^{1/3}\right), \quad \text{(A52)}$$
$$C_E = D[1 - \exp(-E_{\rm proj}/T_l)] - 0.292 \exp\left(-E_{\rm proj}/792\right) \cos\left(0.229 E_{\rm proj}^{0.453}\right), \quad \text{(A53)}$$

where $D = 2.05$, and

for proton-induced reactions,

$$T_l = 40 \text{ for } A_{\rm proj} < 120,$$
$$T_l = 80 \text{ for } A_{\rm proj} \geqslant 120,$$

for neutron-induced reactions,

$$T_l = 30 \text{ for } 11 \leqslant A_{\rm proj} \leqslant 40,$$
$$T_l = 40 \text{ for } A_{\rm proj} < 11 \text{ and } A_{\rm proj} > 40.$$

For $A_{\rm proj} < 200$

$$\chi_{\rm m} = 1 - \chi_l \exp\left[-E_{\rm proj}/(\chi_l S_l)\right], \quad \text{(A54)}$$

with

$$\chi_l = 2.83 - 3.1 \times 10^{-2} A_{\rm proj} + 1.7 \times 10^{-4.} A_{\rm proj}^2, \quad \text{(A55)}$$

TABLE III. Constants used in SPACS for the parameterization of structural effects.

Parameter	Constant	Value
Neutron width strength	C_n	0.0055
γ-ray competition strength	C_γ	0.6
Influence of L	J_{cr}	5
	D_J	1

and

$$\begin{aligned} S_l &= 0.6 \quad \text{for} \quad A_{\text{proj}} < 12, \\ S_l &= 1.6 \quad \text{for} \quad A_{\text{proj}} = 12, \\ S_l &= 1.0 \quad \text{for} \quad A_{\text{proj}} > 12. \end{aligned}$$

For $A_{\text{proj}} \geqslant 200$,

$$\chi_{\text{m}} = \{1 - 0.3\exp[-(E_{\text{proj}} - 1)/15]\} \times [1 - \exp(0.9 - E_{\text{proj}})]. \quad \text{(A56)}$$

5. Numerical values of the parameters

The constants entering into the SPACS parameterization were adjusted empirically along the comparison with experimental data, mostly based on the GSI measurements due to their completeness. The parameters required to compute the spallation-residue mass yield are gathered in Table I, those of the charge-dispersion curve are summarized in Table II, whereas Table III concerns the modeling of structural effects.

For the formalism of charge dispersion, wherever additional terms have been introduced to the fragmentation parameterization EPAX, for the sake of spallation, the numerical values of the EPAX3 parameters have been re-adjusted. The value of some specific parameters in II can thus differ from what reported in Table 1 of Ref. [27].

As noted previously, the prescriptions developed along this work for the width parameter R in Eqs. (A21)–(A26) and for the modeling of structural effects in Eqs. (A35)–(A45) are rather general, independent of the reaction mechanism. It may thus be worth implementing them in other empirical analytical models and, namely, in EPAX for fragmentation.

[1] http://www.isolde.web.cern.ch/
[2] http://www.orau.org/ria/
[3] http://www.triumf.ca/research/research-facilities/
[4] C. D. Bowman *et al.*, Nucl. Instrum. Methods Phys. Res., Sect. A **320**, 336 (1992).
[5] H. Ait Abderrahim *et al.*, Nucl. Instrum. Methods Phys. Res., Sect. A **463**, 487 (2001).
[6] C. J. Waddington *et al.*, Adv. Space Res. **15**, 39 (1995).
[7] D. Schardt, T. Elsässer, and D. Schulz-Ertner, Rev. Mod. Phys. **82**, 383 (2010).
[8] http://www-ap.fnal.gov/MARS
[9] T. Goorley *et al.*, Nucl. Technol. **180**, 298 (2012).
[10] A. Fasso *et al.*, CERN-2005-10, INFN/TC_05/11, SLAC-R-773.
[11] A. Boudard, J. Cugnon, S. Leray, and C. Volant, Phys. Rev. C **66**, 044615 (2002).
[12] A. Kelic, M. V. Ricciardi, and K.-H. Schmidt, arXiv:0906.4193 [nucl-th].
[13] I. V. Moskalenko, S. G. Mashnik, and A. W. Strong, arXiv:astro-ph/0106502.
[14] R. Silberberg and C. H. Tsao, Astrophys. J., Suppl. Scr. **25**, 315 (1973).
[15] G. Rudstam and Z. Naturforschg. Teil A **21**, 1027 (1966).
[16] W. R. Webber, J. C. Kish, and D. A. Schrier, Phys. Rev. C **41**, 520 (1990); **41**, 566 (1990).
[17] C. J. Waddington J. R. Cummings, B. S. Nilsen, and T. L. Garrard, Phys. Rev. C **61**, 024910 (2000).
[18] N. T. Porile, G. D. Cole, and C. R. Rudy, Phys. Rev. C **19**, 2288 (1979).
[19] H. Yashima, Y. Uwamino, H. Sugita, T. Nakamura, S. Ito, and A. Fukumura, Phys. Rev. C **66**, 044607 (2002).
[20] H. Boggild and T. Ferbel, Annu. Rev. Nucl. Sci. **24**, 451 (1974).
[21] C. H. Tsao, R. Silberberg, A. F. Barghouty, I. Sihver, and T. Kanai, Phys. Rev. C **47**, 1257 (1993).
[22] J. C. Hill, F. K. Wohn, J. A. Winger, M. Khayat, M. T. Mercier, and A. R. Smith, Phys. Rev. C **39**, 524 (1989).
[23] L. Y. Geer, J. Klarmann, B. S. Nilsen, C. J. Waddington, W. R. Binns, J. R. Cummings, and T. L. Garrard, Phys. Rev. C **52**, 334 (1995).
[24] J. R. Cummings, W. R. Binns, T. L. Garrard, M. H. Israel, J. Klarmann, E. C. Stone, and C. J. Waddington, Phys. Rev. C **42**, 2530 (1990).
[25] K. Sümmerer, Nucl. Instrum. Methods Phys. Res., Sect. B **204**, 278 (2003).
[26] K. Sümmerer and B. Blank, Phys. Rev. C **61**, 034607 (2000).
[27] K. Sümmerer, Phys. Rev. C **86**, 014601 (2012).
[28] X. H. Zhang, Nucl. Phys. A **915**, 59 (2013).
[29] C. Villagrasa-Canton *et al.*, Phys. Rev. C **75**, 044603 (2007).
[30] S. G. Mashnik, K. K. Gudima, and M. I. Baznat, arXiv:nucl-th/0603046.
[31] C. N. Knott *et al.*, Phys. Rev. C **53**, 347 (1996).
[32] X. Campi and J. Hüfner, Phys. Rev. C **24**, 2199 (1981).
[33] J.-P. Dufour, Nucl. Phys. A **387**, 157c (1982).
[34] L. C. Moretto, Nucl. Phys. A **216**, 1 (1973).
[35] Experimental Nuclear Reaction Data (EXFOR) database [http://www-nds-iaea.org/exfor/exfor00.htm].
[36] R. Serber, Phys. Rev. **72**, 1114 (1947).
[37] K. K. Gudima, S. G. Mashnik, and V. D. Toneev, Nucl. Phys. A **401**, 329 (1983) and Communications JINR, P2-80-774 and P2-80-777, Dubna, USSR, 1980.
[38] S. G. Mashnik *et al.*, IAEA Report No. INDC(NDS)-0530, 2008 (unpublished).
[39] J. Cugnon, C. Voland, and S. Vuillier, Nucl. Phys. A **620**, 475 (1997).
[40] V. E. Bunakov, L. V. Krasnov, and A. V. Fomichev, Eur. Phys. J. A **8**, 447 (2000).
[41] K. Sümmerer, W. Brüchle, D. J. Morrissey, M. Schädel, B. Szweryn, and Y. Welfan, Phys. Rev. C **42**, 2546 (1990).
[42] A. Schuettauf *et al.*, Nucl. Phys. A **607**, 457 (1996).
[43] M. V. Ricciardi, A. V. Ignatyuk, A. Kelic, P. Napolitani, F. Rejmund, K.-H. Schmidt, and O. Yordanov, Nucl. Phys. A **733**, 299 (2004).

[44] R. K. Tripathi, J. W. Wilson, and F. A. Cucinotta, Nucl. Instrum. Methods Phys. Res., Sect. B **129**, 11 (1997).
[45] R. K. Tripathi, F. A. Cucinotta, and J. W. Wilson, Nucl. Instrum. Methods Phys. Res., Sect. B **117**, 347 (1996).
[46] J.-P. Gaimard and K.-H. Schmidt, Nucl. Phys. A **531**, 709 (1991).
[47] R. J. Charity, Phys. Rev. C **58**, 1073 (1998).
[48] F. Rejmund *et al.*, Nucl. Phys. A **683**, 540 (2001).
[49] M. V. Ricciardi *et al.*, arXiv:1007.0386.
[50] A. Kelic, K.-H. Schmidt, T. Enqvist, A. Boudard, P. Armbruster, J. Benlliure, M. Bernas, S. Czajkowski, R. Legrain, S. Leray, B. Mustapha, M. Pravikoff, F. Rejmund, C. Stephan, J. Taieb, L. Tassan-Got, C. Volant, and W. Wlazlo, Phys. Rev. C **70**, 064608 (2004).
[51] J. Su, F.-S. Zhang, and B.-A. Bian, Phys. Rev. C **83**, 014608 (2011).
[52] I. Lombardo *et al.*, Phys. Rev. C **84**, 024613 (2011).
[53] G. Ademard *et al.*, Phys. Rev. C **83**, 054619 (2011).
[54] J. X. Cheng, X. Jiang, S. W. Yan, and D. H. Zhang, J. Phys. G: Nucl. Part. Phys. **39**, 055104 (2012).
[55] M. D'Agostino, M. Bruno, F. Gulminelli, L. Morelli, G. Baiocco, L. Bardelli, S. Barlini, F. Cannata, G. Casini, E. Geraci, F. Gramegna, V. L. Kravchuk, T. Marchi, A. Moroni, A. Ordine, and A. R. Raduta, Nucl. Phys. A **875**, 139 (2012).
[56] G. Casini *et al.*, Phys. Rev. C **86**, 011602(R) (2012).
[57] O. B. Tarasov *et al.*, Phys. Rev. C **87**, 054612 (2013).
[58] D. Henzlova *et al.*, Phys. Rev. C **78**, 044616 (2008).
[59] L. Giot *et al.*, Nucl. Phys. A **899**, 116 (2013).
[60] J. Hüfner, C. Sander, and G. Wolschin, Phys. Lett. B **73**, 289 (1978).
[61] A. Bohr and B. R. Mottelson, in *Nuclear Structure* (W. A. Benjamin, Inc, New York, 1969), Vol. 1.
[62] S. Leray *et al.*, J. Korean Phys. Soc. **59**, 791 (2011).
[63] M. Wang, G. Audi, A. H. Wapstra, F. G. Kondev, M. MacCormick, X. Xu, and B. Pfeiffer, CPC (HEP&NP) **36**, 1603 (2012).
[64] W. D. Myers and W. J. Swiatecki, Nucl. Phys. A **601**, 141 (1996).
[65] B. Mei *et al.*, Phys. Rev. C **89**, 054612 (2014).
[66] A. V. Ignatyuk, *Proceedings of the Conference Bologna* 2000 Structure of the Nucleus at the Dawn of the Century, Bologna, Italy, 2000 (World Scientific, Singapore, 2001).
[67] T. von Egidy and D. Bucurescu, Phys. Rev. C **80**, 054310 (2009).
[68] M. De Jong, A. V. Ignatyuk, and K.-H. Schmidt, Nucl. Phys. A **613**, 435 (1997).
[69] Y. Yariv and Z. Fraenkel, Phys. Rev. C **20**, 2227 (1979).
[70] T. Enqvist *et al.*, Nucl. Phys. A **686**, 481 (2001).
[71] B. Fernandez-Dominguez *et al.*, Nucl. Phys. A **747**, 227 (2005).
[72] J. Benlliure *et al.*, Nucl. Phys. A **700**, 469 (2002).
[73] P. Napolitani, K.-H. Schmidt, and L. Tassan-Got, J. Phys. G Nucl. Part. Phys. **38**, 115006 (2011).
[74] L. Audouin *et al.*, Nucl. Phys. A **768**, 1 (2006).
[75] M. Gloris *et al.*, Nucl. Instrum. Methods Phys. Res., Sect. A **463**, 593 (2001).
[76] L. Tassan-Got and C. Paradela, EURATOM Research and Training Programme on Nuclear Energy within the 6th Framework Programme (2002) (unpublished); C. Paradela *et al.*, Final Activity Report, Spallawaste Project, Contract No. 016733 (unpublished).
[77] P. Napolitani *et al.*, Phys. Rev. C **76**, 064609 (2007).
[78] P. Napolitani, K.-H. Schmidt, A. S. Botvina, F. Rejmund, L. Tassan-Got, and C. Villagrasa, Phys. Rev. C **70**, 054607 (2004).
[79] C. N. Knott *et al.*, Phys. Rev. C **56**, 398 (1997).
[80] C.-X. Chen *et al.*, Phys. Rev. C **56**, 1536 (1997).
[81] M. Epherre and E. Gradsztajn, J. Phys. (Paris) **28**, 745 (1967).
[82] D. L. Olson, B. L. Berman, D. E. Greiner, H. H. Heckman, P. J. Lindstrom, and H. J. Crawford, Phys. Rev. C **28**, 1602 (1983).
[83] P. M. Epherre and C. Seide, Phys. Rev. C **3**, 2167 (1971).
[84] J. Dudouet *et al.*, Nucl. Instrum. Methods Phys. Res., Sect. A **98**, 715 (2013).
[85] J. Dudouet *et al.*, Phys. Rev. C **88**, 024606 (2013).
[86] S. B. Kaufman and E. P. Steinberg, Phys. Rev. C **22**, 167 (1980).
[87] Y. E. Titarenko, ISTC Project No. 3266, Final Technical Report, 2010 (unpublished).
[88] Y. E. Titarenko *et al.*, Nucl. Instrum. Methods Phys. Res., Sect. A **414**, 73 (1998).
[89] Y. E. Titarenko *et al.*, Phys. Rev. C **84**, 064612 (2011).
[90] I. Leya, H. Busemann, H. Baur, R. Wieler, M. Gloris, S. Neumann, R. Michel, F. Sudbrock, and U. Herpers, Nucl. Instrum. Methods Phys. Res., Sect. B **145**, 449 (1998).
[91] B. I. Belyaev, A. V. Kalyamin, and A. N. Murin, J BAS **27**, 907 (1963).
[92] C. Scheidenberger *et al.*, Phys. Rev. C **70**, 014902 (2004).
[93] N. Barghouty (private communication).
[94] T. Toshito *et al.*, Phys. Rev. C **75**, 054606 (2007).
[95] S. G. Mashnik and A. J. Sierk, arXiv:nucl-th/0011064.
[96] I. V. Moskalenko and S. G. Mashnik, *Proceedings of the 28th International Cosmic Ray Conference, Tsukuba, Japan, 2003*, edited by T. Kajita, Y. Asaoka, A. Kawachi, M. Sasaki, and Y. Matsubara (Universal Academy Press, Tokyo, 2003), p. 1969.
[97] A. Boudard, J. Cugnon, J.-C. David, S. Leray, and D. Mancusi, Phys. Rev. C **87**, 014606 (2013).